INFORMATION TO USERS

This manuscript has been reproduced from the microfilm master. UMI films the text directly from the original or copy submitted. Thus, some thesis and dissertation copies are in typewriter face, while others may be from any type of computer printer.

The quality of this reproduction is dependent upon the quality of the copy submitted. Broken or indistinct print, colored or poor quality illustrations and photographs, print bleedthrough, substandard margins, and improper alignment can adversely affect reproduction.

In the unlikely event that the author did not send UMI a complete manuscript and there are missing pages, these will be noted. Also, if unauthorized copyright material had to be removed, a note will indicate the deletion.

Oversize materials (e.g., maps, drawings, charts) are reproduced by sectioning the original, beginning at the upper left-hand corner and continuing from left to right in equal sections with small overlaps.

Photographs included in the original manuscript have been reproduced xerographically in this copy. Higher quality 6" x 9" black and white photographic prints are available for any photographs or illustrations appearing in this copy for an additional charge. Contact UMI directly to order.

UMI®

University of Alberta

Fluid-Absent Melting of High-Grade Semi-Pelites: P-T Constraints on Orthopyroxene Formation and Implications for Granulite Genesis

by

Rajeev Kumar Sasidharan Nair ©

A thesis submitted to the Faculty of Graduate Studies and Research in partial fulfillment of the requirements of *Master of Science*

Department of Earth and Atmospheric Sciences

Edmonton, Alberta
Fall 2000

0-612-59874-8

Canada

University of Alberta

Library Release Form

Name of Author: Rajeev Kumar Sasidharan Nair

Title of Thesis: Fluid-absent Melting of High-Grade Semi-pelites: P-T Constraints on Orthopyroxene Formation and Implications for Granulite Genesis.

Degree: Master of Science

Year this Degree Granted: 2000

Rajeev Sasidharan Nair
"Aswathy"
Pachalloor P.O
Trivandrum, Kerala
INDIA 695027

Date: 26 September, 2000.

"………arguments such as '*the reaction has been calibrated already*' are not sufficient reasons to avoid repeating experiments. The operative questions must be '*how well should we know this reaction?*'…".

McKenna and Hodges (1988)
American Mineralogist v. 73.
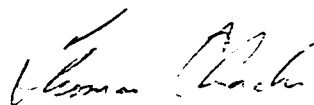
Abstract

The fluid-absent melting behavior of two, natural high-grade semi-pelitic rocks were studied using a piston-cylinder apparatus in the P-T range 7-15 kbar and 800-1050° C. The aim was to constrain P-T conditions required for the formation of orthopyroxene, the metamorphic index mineral marking the transition from the amphibolite to the granulite facies. The starting materials (garnet-biotite-gneiss) were obtained from a transitional amphibolite-granulite terrane in order to simulate closely the transition process in nature. The results indicate that temperatures >875° – 900° C are required to stabilize orthopyroxene in rocks of semi-pelitic bulk compositions under fluid-absent conditions at mid-to-lower crustal depths. Such high temperatures conflict with the temperature estimates obtained in transitional amphibolite-granulite terranes using Fe-Mg exchange thermometers, implying either that these thermometers record temperatures much below the peak metamorphic temperature or that regional granulite formation occurs through a process other than fluid-absent melting.
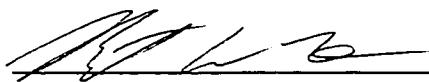
University of Alberta

Faculty of Graduate Studies and Research

The undersigned certify that they have read, and recommend to the Faculty of Graduate Studies and Research for acceptance, a thesis entitled **Fluid-Absent Melting of High-Grade Semi-Pelites: P-T constraints on Orthopyroxene Formation and Implications for Granulite Genesis** submitted by Rajeev Kumar Sasidharan Nair in partial fulfillment of the requirements for the degree of Master of Science.

Dr. Thomas Chacko (Supervisor)

Dr. Robert Luth (Committee Member)

Dr. Doug Schmitt (Committee Member)

Date

Dedication

To my father

for all the things you did for me
and
for all the things I couldn't do for you

To my mother

for me not being there
and
for letting me pursue what I like

To my sisters

for growing so old when still young

Acknowledgements

This thesis would never be anywhere close to what it is now without the support I received from a lot of people who at different stages walked into my life and it is impossible to mention the name of all in such a short space. However, no space constraints should prevent me from expressing my deep gratitude to my supervisor Dr. Tom Chacko for his inspiring guidance, patience and wisdom. His ardent interest in the project was very much instrumental in its successful completion. I am also very much indebted to him and his family for the brotherly care they gave me during one of the most testing times of my life (I will never forget Jacob giving up his bed for me with the words "it is really warm". I certainly needed it that night. Thank you). No superlatives could describe how helpful a supervisor, Tom is.

Dr. Robert Luth is thanked for providing valuable advice in doing experiments and for giving me free reign in his laboratory and access to all the facilities (and thanks very much for treating me like your own student and offering an office in the lab where I could hide and write). But for the great working environment and easy access to the facilities at the Chris Scarfe Experimental Petrology lab this project would be far from completion. I would also like to thank Dr. Doug Schmitt for his comments on the thesis.

Lang Shi trained and assisted me in using the electron microprobe on which almost all the analytical work was done and is thanked sincerely for all his help. Ken Domanik was the lab manager when I did most of my experiments and his efficiency in quickly meeting my laboratory requirements is very much appreciated. Diane "the safety" Caird provided technical assistance in X-ray lab and with various other things in the experimental petrology lab. Don Resultay and Mark Labbe are thanked for their help in the thin-section laboratory. George Braybrook is thanked for his assistance with SEM imaging.

I almost dropped out of this program even before I started as my arrival in Edmonton was soon followed by a family crisis. Tom, Leslie, Suman, George, Jeanu

chechi, Asha and Seeth Seethram – your support during that time made my decision to come back much easier. Dr. Santosh – I am indebted to you the way you arranged for my return to India and the words of encouragement you gave to me and my family during that time. You have always treated me as your brother and your support at that time was truly befitting one. I was in a emotional and financial hole at that time and was helped out of it by my friends Satish Kumar, Rajesh H.M, Rajesh Chandran, Shaju and Bindu. I am grateful for your help.

Dr. Santosh is also thanked for keeping my interests in geology alive. But for the time I spent in his lab after I finished my first masters degree in India, I would be doing something else. People like Dr. Chacko and Dr. Luth continue to inspire me to do more research in a field where results and returns are hard to come. The financial help I received from the Department of Earth and Atmospheric Sciences in the form of Teaching Assistantship and Research Assistantship is gratefully acknowledged. The project also received invaluable financial support through, an NSERC grant (to Tom Chacko), Chris Scarfe Memorial Graduate Scholarship, and J Gordin Kaplan Graduate Student award.

Once you meet the requirements like having an able supervisor and adequate funding, the next best thing a graduate student could hope for is to be surrounded by great friends. I am certainly fortunate to have had plenty of them. Jen Unterschutz, Leslie Driver, Ram Maikala, Suman De, Poulomi Sannigrahi, Cathy Skilliter, Nikhil Rao, Pedro Jugo, Elisabeth Ronacher, Andrea Noyes, Murray Gingras, Karen Fallas, Candice Stuart, Karen Heppenstall, David Selby, Louise Byass, Surajlal and Kaia Kjar are all great friends who have cheered me up many times during my stay in Edmonton. It certainly makes it easy to leave one's family and to be in a foreign country when people like these are around. My acquaintance with these people has taught me valuable lessons in academics and life. Mrs. Joyce Harries treated me like her son for more than two years. The wholesome breakfast she served me every morning kept me warm even during the coldest winter days.

I am also fortunate to have another great force supporting my pursuits in life- the prayers of my family. My father took great troubles to see that I never had to worry too much about getting whatever things I wanted (even when some of those things were not absolutely essential). But for his support I wouldn't be studying in Canada. He once wrote to me " I want you to reach a high academic position which I couldn't get". The selfless attitude and compassion he extended towards others was perhaps the earliest lessons that I was exposed to in life. I am sure he would be proud to know that the people he left behind are holding on to his beliefs. My mother and sisters never wanted me to return to India to stay with them, even though I was able to feel their need to have me beside them. They showed great courage in beginning a new life three years ago, without seeing two people they were so used to seeing every day. I am really thankful to the three of you (Amma, Vidhya and Rani) for letting me pursue my studies. I am fortunate to have you as my family and hope that all your prayers will be answered soon.

Table of Contents

List of Tables

List of Figures

Abbreviations

A/CNK	molecular proportion of $(Al_2O_3/CaO+Na_2O+K_2O)$
Bio	Biotite
Grt	Garnet
Ilm	Ilmenite
KAL	Kalanjur
Kfs	Alkali-feldspar
M	Quenched melt
Mg-number	molar $(Mg/Mg+Fe)$
n.a.	not analysed
o.d.	outer diameter
Opx	Orthopyroxene
p.f.u.	atoms per formula unit
P	Pressure
Plg	Plagioclase
PON	Ponmudi
Py	Pyrrhotite
QFM	Quartz-Fayalite-Magnetite buffer reaction
Qtz	Quartz
Ru	Rutile
T	Temperature
wt. %	weight percent

Introduction

Partial melting of pre-existing rocks is believed to be a major process in the formation and differentiation of continental crust. The results of this process range from millimetre- to centimetre-scale leucosomes in migmatites to large granitoid batholiths, such as are found at plate margins. These extremes in the outcome of partial melting represent progressive stages in the production and segregation of melt from its source rock. It is generally believed that partial melting occurs under fluid-deficient or fluid-absent (no free fluid phase present) conditions (e.g., Clemens and Vielzeuf, 1987). The generation of melts from crustal rocks under these conditions has been variously described as "vapor-absent melting" (Rutter and Wyllie, 1988), "dehydration melting" (Thompson, 1982) or "fluid-absent melting" (Clemens, 1984), and involves the breakdown of a hydrous mineral-bearing assemblage into a less hydrous or anhydrous assemblage and an H_2O-undersaturated melt. The operation of this process on a large scale can lead to intra-crustal differentiation through the emplacement of the melt at upper crustal levels, leaving behind an anhydrous, granulite-facies residue in the lower crust. Thus, fluid-absent melting of crustal protoliths may play a major role in the development of granulite-facies mineral assemblages (Fyfe, 1973; Clemens, 1992; Clemens et al., 1997). Studying the phase equilibria of fluid-absent melting is critical then, for understanding the formation of both granulites and granites, and establishing unambiguously the connection between the two.

There have been a number of excellent experimental studies examining the fluid-absent melting behavior of typical crustal rock types (e.g., Vielzeuf and Holloway, 1988; Le Breton and Thompson, 1988; Patiño Douce and Johnston, 1991; Skjerlie and Johnston, 1993; Skjerlie et al., 1993; Vielzeuf and Montel, 1994; Patiño Douce and Beard, 1995,1996; Stevens et al., 1997; Patiño Douce and Harris, 1998; Pickering and Johnston, 1998). The majority of these studies were aimed at investigating the fertility (melt productivity) of common crustal rock types under fluid–absent conditions or at constraining the composition of the melts generated from such rocks. Although these studies were useful in developing the general topology of the fluid-absent solidus for typical crustal rocks, very few specifically investigated the pressure-temperature conditions required for the formation of anhydrous mafic phases during the melting process. One of the most significant mineralogical transformations that occur under high-grade metamorphic conditions is the stabilization of the anhydrous mineral orthopyroxene (opx) at the expense of hydrous minerals, biotite and hornblende. In rocks of semi-pelitic or granitic bulk composition, the opx-in isograd marks the transition from amphibolite-facies to granulite-facies conditions. Quantification of the P-T conditions at which opx first appears in these rocks would enhance our understanding of the granulite-forming process and also provide a P-T constraint that is directly applicable in the field. The main objective of this study is to determine the P-T conditions required for opx formation in semi-pelitic rocks by the process of fluid-absent melting.

The rationale for the present study stems from observations made regarding the composition of hydrous minerals in rocks undergoing amphibolite- to granulite-facies transition. Being dependent on the release of water stored in hydrous phases, the fluid-absent melting process is essentially a measure of the stability of hydrous phase(s) under fluid-absent conditions. Therefore, any compositional variable that affects the stability of hydrous phase(s) may affect the P-T position of fluid-absent melting reactions. Two elements known to stabilize biotite to higher temperature are Ti and F (Forbes and Flower, 1974; Trønnes et al., 1985; Peterson et al., 1991; Patiño Douce, 1993; Dooley and Patiño Douce, 1996). Figure 1A compares the Ti content and Mg-number (molar Mg/(Mg+Fe)) of biotites from several transitional amphibolite-granulite terranes with those used in previous experimental melting studies on pelitic and semi-pelitic bulk compositions. Although not an exhaustive compilation, the figure illustrates the Ti-rich nature of transitional terrane biotites in comparison to those used in previous melting experiments. Similarly, transitional terrane biotites are generally higher in F relative to ones used in previous experimental studies (Fig. 1B). Thus, it is possible that biotites from these transitional terranes are stable to higher temperatures than indicated by earlier experiments.

A

Ti p.f.u. (based on 22 O)

- □ Transitional terranes
- ▲ Previous experiments
- ● This Study

B

F p.f.u. (based on 22 O)

- □ Transitional terranes
- ▲ Previous experiments
- ● This Study

$Mg/(Mg+Fe^T)$ (molar)
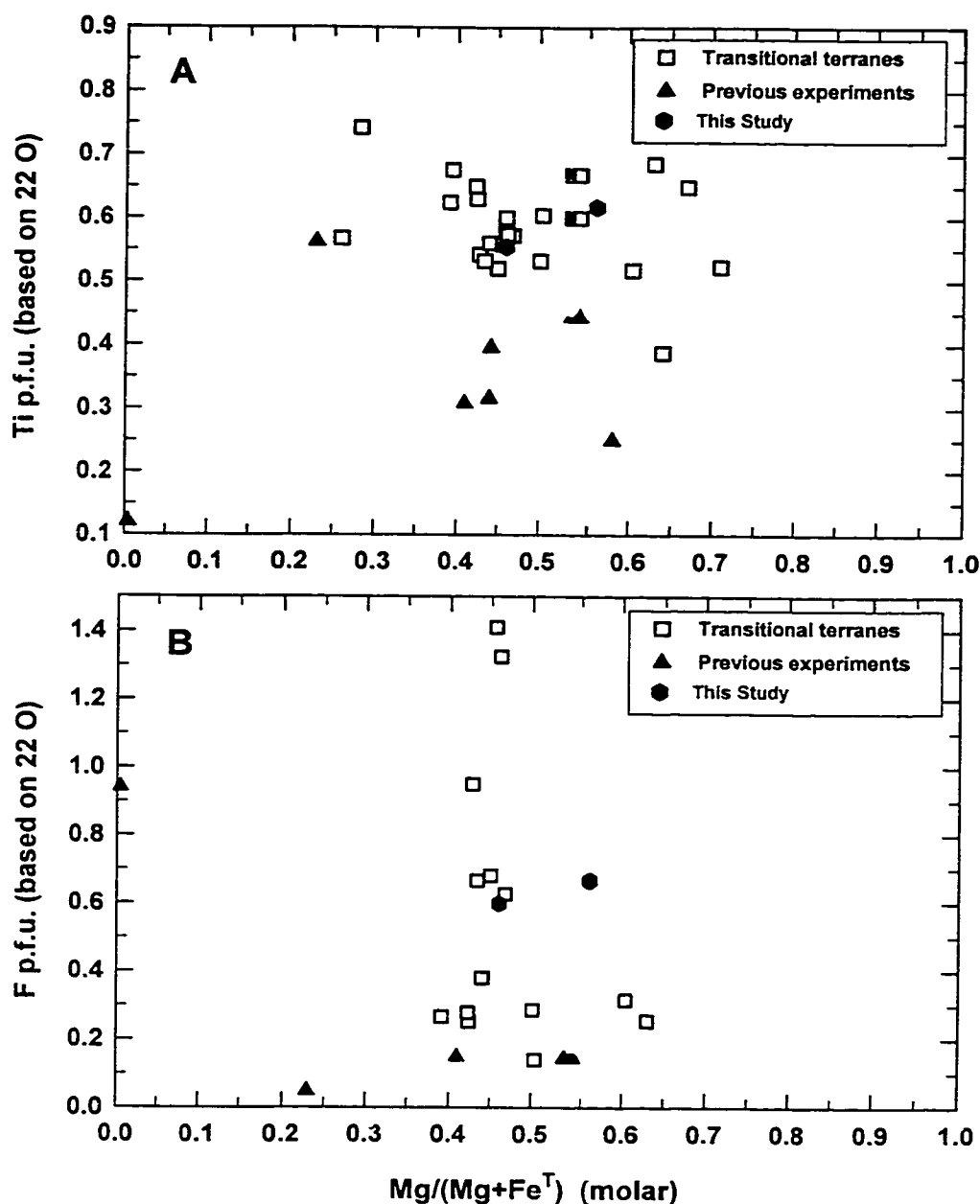
Figure 1. Comparison of biotite compositions from amphibolite-granulite transitional terranes with those used in previous experimental studies. **A.** Ti vs. $Mg/(Mg + Fe^T)$. **B.** F vs. $Mg/(Mg + Fe^T)$. Transitional terrane data from: South India - Janardhan et al. (1982), Hansen et al. (1987); Sri Lanka - Hansen et al. (1987), Burton and O'Nions (1990); Antarctica - Santosh and Yoshida (1992); Uusimaa, Finland - Schreurs (1985); Seiland Province, Norway - Elvevold et al. (1994); Ivrea zone, Italy - Franz and Harlov (1998); Wayah, U.S.A - Eckert et al. (1989); Reading Prong, U.S.A. - Young (1995); Wyoming, U.S.A. - Grant and Frost (1990); Quetico subprovince, Canada - Pan et al. (1994); and Slave Province, Canada - Chacko (pers. comm.). Experimental biotites – Le Breton and Thompson (1988), Patino Douce and Johnston (1991), Vielzeuf and Montel (1994), Patino Douce and Beard (1995,1996), and Stevens et al. (1997).

4

The disparity in experimental and natural biotite compositions described above reflects the fact that many of the starting materials used in earlier experimental studies were taken from (or have mineral compositions typical of) mid- to upper-amphibolite-facies terranes rather than transitional amphibolite-granulite terranes. I suggest that an experimental study using rocks from transitional terranes would more closely simulate the fluid-absent melting process occurring in nature and thereby provide a better understanding of phase relations under high-grade conditions. This paper presents the results of fluid-absent melting experiments on two high-grade semi-pelitic rocks and focuses on constraining the P-T conditions required for the first appearance of opx in these rocks.

Methods

Starting Materials

In accord with the above arguments, the starting materials for the experiments in this study were rocks that are known from field relations to have been metamorphosed to near granulite-facies conditions. The starting materials were obtained from two localities, Ponmudi and Kalanjur, from the high-grade metasedimentary terrane of south India commonly referred to as the Kerala Khondalite Belt (KKB). The KKB is dominated by garnet-biotite ± opx ± graphite gneisses (semi-pelites), and garnet-biotite-sillimanite ± cordierite gneisses (pelites), intercalated with minor amounts of mafic

granulites, calc-silicates and quartzites (Chacko et al., 1987; Chacko et al., 1992). These mineral assemblages indicate uppermost amphibolite- to granulite-facies metamorphic conditions throughout the KKB. Ponmudi and Kalanjur are two of the many localities in KKB that record the nature of the granulite-forming process. At these localities, the granulite is developed as patches and veins that partially overprint the fabric of the host garnet-biotite gneiss (Fig. 2) (Ravindra Kumar et al., 1985; Srikantappa et al., 1985; Ravindra Kumar and Chacko, 1986). Close observation of the granulite patches shows that they crosscut and largely obliterate the gneissic foliation. In places, however, relict gneissic foliation can be traced through the patches. The gneissic and granulitic portions of the outcrop are virtually identical in their major-element compositions but differ mineralogically in that the granulite contains opx and significantly less biotite than the gneiss (Ravindra Kumar and Chacko, 1986). These mineralogical, geochemical and field relationships strongly suggest that garnet-biotite gneiss was the lithological precursor to the granulite. Moreover, the intimate spatial association of the two rock types requires that they were metamorphosed at very similar P-T conditions, and specifically P-T conditions that verged on that necessary to produce granulite-facies mineral assemblages. The opx-free gneiss at these localities would, therefore, serve as ideal starting materials for investigating P-T conditions of opx formation by fluid-absent melting of high-grade rocks.
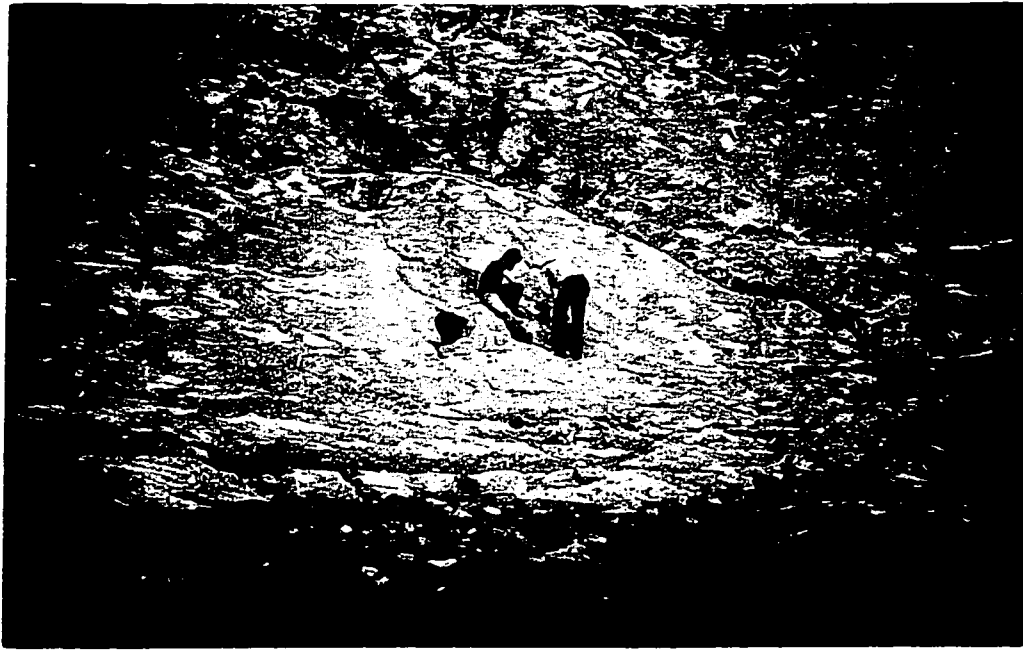
Figure 2A. Quarry at Ponmudi, south India showing patchy development of granulite (green) within the host garnet-biotite gneiss (white).

Figure 2B. Close view of a granulite patch at Ponmudi. Note the obliteration of the gneissic foliation against the granulite patch. The foliation however is faintly preserved in some areas within the granulite. Starting material for the present experiments was taken from the light colored portion (garnet-biotite gneiss) of the outcrop.

7

Table 1. Composition of the starting materials.

Wt %	SiO$_2$	TiO$_2$	Al$_2$O$_3$	FeO^T	MnO	MgO	CaO	Na$_2$O	K$_2$O	F	Cl	Total	Mg-no.*
Ponmudi													
Biotite	37.58	5.02	13.76	21.88	0.03	10.62	0.01	0.12	10.21	1.26	0.32	100.81	46
Plagioclase	59.31	n.a.	24.68	0.03	0.01	0.00	6.61	7.66	0.27	n.a.	n.a.	98.57	
K-feldspar	64.87	0.02	18.73	0.01	0.00	0.00	0.14	1.63	14.04	n.a.	n.a.	99.44	
Garnet	37.20	0.05	21.29	34.85	0.68	3.69	2.53	0.00	n.a.	n.a.	n.a.	100.29	16
Ilmenite	0.01	52.30	n.a.	47.63	0.07	0.03	0.03	n.a.	n.a.	n.a.	n.a.	100.07	
Kalanjur													
Biotite	35.87	5.45	13.62	17.38	0.02	12.63	0.01	0.11	9.60	1.40	0.35	96.44	56
Plagioclase	58.25	n.a.	25.49	0.03	0.01	0.01	7.63	7.03	0.24	n.a.	n.a.	98.69	
K-feldspar	64.66	0.05	18.99	0.01	0.01	0.00	0.37	2.22	12.91	n.a.	n.a.	99.22	
Garnet	37.73	0.04	21.73	32.40	0.67	6.13	1.81	0.01	n.a.	n.a.	n.a.	100.54	25
Ilmenite	0.03	52.30	n.a.	46.15	0.19	0.02	0.02	n.a.	n.a.	n.a.	n.a.	98.69	
Bulk composition† (wt%)													
Ponmudi	68.80	0.83	14.60	5.99	0.08	1.05	2.13	2.55	4.42	n.a.	n.a.	100.45	23
Kalanjur	68.00	0.94	14.40	6.22	0.11	1.56	2.45	2.40	3.63	n.a.	n.a.	99.71	31

* - molar (Mg/Fe^T+Mg)x 100, T- total Fe reported as FeO, n.a.- not analysed, †- from Chacko (1987).

8

The compositions of the starting materials are shown in Table 1 and are discussed individually below.

Ponmudi

The garnet-biotite gneiss from Ponmudi (hereafter called PON) contains about 10% biotite, 30% quartz, 28% plagioclase (An_{32}), 14% alkali-feldspar, 16% garnet and <2% ilmenite. The rock is peraluminous (A/CNK = 1.15) but Al_2SiO_5-undersaturated, similar to a metagraywacke. The biotite in this starting material contains 5.0 wt. % TiO_2 and 1.3 wt. % F and has a Mg-number of 0.46. The high Ti and F content of this biotite are generally representative of biotites from other prograde transitional amphibolite-granulite terranes. The garnet is almandine rich (77 mol % almandine, 15 mol % pyrope) with relatively low grossular content (7 mol %).

Kalanjur

The Kalanjur starting material (hereafter called KAL) is very similar to PON in terms of mineralogy. It contains about 11% biotite, 30% quartz, 30% plagioclase, 10% alkali-feldspar, 18% garnet and <1% ilmenite. The rock is peraluminous (A/CNK = 1.18) and Al_2SiO_5-undersaturated, as is the case with PON. The biotite in KAL is more magnesian (Mg-number = 0.56) and slightly more Ti- and F-rich (5.4 and 1.4 wt. %, respectively) than the biotite in PON. The plagioclase is also more anorthitic (X_{An} = 37 mol %) than that in PON.

Garnet is an almandine-pyrope solid solution (70 mol % almandine and 24 mol % pyrope) with minor grossular component (5 mol %).

As the focus of the study was not to investigate the fertility of any particular rock type under fluid-absent conditions, the starting materials were not intended to mimic any common crustal rock type, although the bulk composition and the composition of the constituent mineral phases of both PON and KAL broadly correspond to those of metagraywackes at high metamorphic grade. The compositions of the starting materials are such that biotite is the phase that limits melt production under fluid-absent conditions. The presence of a Ti-saturating phase (ilmenite) in both starting materials provides an opportunity to study the variation of Ti in biotite as a function of pressure and temperature.

Experimental Procedures

All experiments were performed under fluid-absent conditions in an end-loaded piston-cylinder apparatus using a 1.91-cm (3/4 inch) –diameter piston. The 4.4 cm long sample assembly consisted of an outer NaCl sleeve and an inner Pyrex glass sleeve containing a tapered graphite furnace (Kushiro, 1976) and crushable ceramic inner parts. The experimental capsules were placed in a ceramic inner sleeve near the center of the graphite furnace. Any free space between the ceramic sleeve and the capsules was filled with Pyrex powder. The NaCl outer sleeve was fired at 300 – 350° C for

approximately one hour prior to use in the experiments. The inner cylinder of the pressure vessel was cleaned to a mirror finish and lightly dusted with dry MoS_2 powder before each experiment. The sample assembly was jacketed with Pb foil prior to insertion into the pressure vessel in order to minimize friction between the assembly and the pressure vessel.

Nominal hydraulic pressures were measured with a Heise bourden tube gauge and converted to sample pressure using a theoretically calculated pressure amplification factor. Correspondence between calculated and true sample pressures was evaluated using the equilibrium Grossular + Quartz = Wollastonite + Anorthite, relative to the P-T position of this equilibrium reported by Windom and Boettcher (1976) and Mattioli and Bishop (1984) (see Appendix 1). These calibration experiments indicated that no pressure correction is required with this sample assembly. The reported pressures are believed to be accurate to within 500 bars. Temperatures were measured with W5Re-W26Re thermocouples. The cold junction of the thermocouple was at laboratory temperature. During the experiments temperature was controlled to within a degree using a solid-state controller (Eurotherm[TM818]), which was run through an Omega ice point. No correction was applied for pressure induced e.m.f. The temperature stability during the runs was within 5° C and the reported temperatures are considered to be accurate within 10° C.

For each experiment the samples were cold pressurized to 2-3 kbar above the desired pressure, and the temperature was then manually increased to that of the desired experimental temperature. Although the

increase in temperature caused decrease in the pressure during run-up, the final experimental conditions was always attained by release of pressure (hot, piston-out technique). The heating procedure was rapid, such that the desired temperature was attained within 10-15 minutes in all experiments. Quenching of the runs were achieved by cutting off the power supply to the furnace, which cooled samples to below 600° C in about 5 seconds. Such a rapid quench rate minimizes the chance of forming quench phases.

In addition to the single-step experiments, reversal experiments (phase reversal) involving a two-step procedure were carried out. In the first step, the starting materials were equilibrated at the P-T conditions where the appearance of the phase of interest (opx) was documented in a previous single-step experiment. During the second step, the temperature of the experiment was lowered while keeping the pressure constant. The criteria for successful reversal include the disappearance of opx and the growth of euhedral biotite crystals. The biotite grains that grew during the reversal experiments also had compositions corresponding to the low temperature.

The starting materials were ground in an agate mortar with distilled water to an average grain size of <10 μm. The powdered material was then treated with dilute HCl to leach away any retrograde chlorite that may have been present in the sample. The samples were rinsed thoroughly with distilled water after the acid treatment and stored in an oven at 120° C for several days before loading the capsules.

Approximately 10 -15 mg of starting material was loaded into 2-mm (o.d.) gold capsules. The small volume of the capsules allowed two capsules to be run in each experiment, one containing the PON and the other the KAL starting material. Considerable care was taken to minimize adsorbed H_2O while loading the capsules. After loading, the capsules were partly crimped and stored in an oven at 120° C for at least 15 hours. The capsules were crimped shut inside the oven and then immediately sealed by arc welding. The capsules were weighed before and after each experiment to detect any weight loss. Experiments with any tear and/or weight loss > 0.1 mg in the capsules were considered unsuccessful and discarded.

The experiments were conducted at temperatures from 800° C to 1000° C at 7 kbar, 875° C to 1050° C at 10 kbar, and 950° C to 1050° C at 15 kbar. The run duration varied from 3 weeks at 800° C to 2 days at 1050° C. The duration of experiments were kept short at high temperatures (>900° C) to minimize any possible desiccation of the samples through diffusion of volatiles through the capsule walls (Patiño Douce and Beard, 1994). The following lines of evidence indicate that significant loss of molecular H_2O did not occur in any of the single-step melting experiments. Firstly, Patiño Douce and Beard (1994) found that H_2O loss from the capsule resulted in an increase in plagioclase abundance at the expense of melt, and formation of high-Ca rims on pre-existing plagioclase grains. In the present experiments, however, the modal abundance of plagioclase decreased, and melt increased with increasing temperature. In addition, the plagioclase grains in the high-

13

temperature experiments were homogenous in composition. Secondly, crystallization of euhedral biotite grains in reversal experiments, which were originally held at much higher temperature, indicates that water remained in the capsule (dissolved in the melt). These results are consistent with the findings of Truckenbrodt and Johannes (1999) who showed that diffusion of molecular H_2O through the capsule walls is not a major problem except in long duration experiments (> 6 days) at temperatures higher than $1000°$ C. The evidence against dissociation of H_2O to H_2 and O_2 and diffusion of H_2 out of the capsule comes from the relatively reduced nature of mineral assemblages in the run products. Calculated $f(O_2)$ values (see below) are at or below the QFM buffer, which precludes significant H_2 loss from the capsule during the experiments as this would have led to more oxidizing conditions.

Analytical Procedures

Capsules from successful experiments were mounted in epoxy and polished. The run products were characterized using a JEOL 8900 electron microprobe at the University of Alberta. Qualitative, energy dispersive techniques were used for phase identification. Quantitative wavelength dispersive analyses of all the phases were performed at an accelerating voltage of 15 kV and a beam current of 15 nA. The beam diameter for the analyses varied between 1 to 3 μm depending on the size of the crystals. A few opx analyses were obtained using a focussed (<1 μm) beam. Natural

14

minerals were used as standards for all the phases (Appendix 2). X-ray intensities were converted to concentrations by means of a ZAF correction routine. The relative proportions of the phases were estimated visually from backscatter electron images.

Redox Conditions

No external oxygen buffers were used in the experiments. However, oxygen fugacity was calculated for all experimental products that contained opx, ilmenite and quartz from the equilibrium

$$2Fe_2O_3 + 4 SiO_2 = 2 Fe_2Si_2O_6 + O_2$$
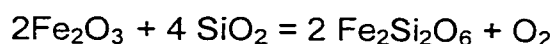
using the standard state properties of Berman (1988) and the solution properties for opx from Sack and Ghiorso (1989) and for ilmenite from Ghiorso (1990). The oxygen fugacity was also calculated from the same equilibrium using the QUIlF program (Anderson et al., 1993). The calculated oxygen fugacities generally range from one-half to two log units below that of the QFM buffer (Table 2). Such values are typical for experimental investigations using piston cylinder assemblies similar to the one employed in the present study (Patiño Douce and Beard, 1995; 1996). The similarity between $f(O_2)$ values calculated for the present experiments with those reported by others facilitates direct comparison with earlier studies.

15

Table 2. Calculated oxygen fugacity values.

Run No.	P (kbar)	T (° C)	log f(O$_2$)[‡]	log f(O$_2$)[†]	ΔQFM[‡]	ΔQFM[†]
RJ-9	7	950	-12.50	-12.72	-1.39	-1.61
RJ-25	7	1000	-10.46	-10.74	-0.12	-0.41
RJ-31	10	1050	-10.45	-10.95	-0.30	-1.58
RJ-10	7	950	-12.29	-13.33	-1.18	-2.22
RJ-26	7	1000	-10.15	-10.62	0.22	-0.28
RJ-32	10	1050	-11.74	-11.77	-1.59	-2.41

‡ calculated using standard state properties of Berman (1988), orthopyroxene solution model of Sack and Ghiorso (1989), and ilmenite solution model of Ghiorso (1990).

† calculated using QUILF program (Anderson et al., 1993).

Results

Description of the run products

The experimental conditions and the phase assemblage observed in the run products are summarized in Table 3.

7 kbar

Trace amounts of melt were observed in the run products of PON and KAL at 800° C, the lowest temperature investigated at this pressure. The amount of biotite in the run products decreased from ~10% at 800° C to less than 1% at 1000° C. This corresponds with an increase in the proportion of garnet, alkali-feldspar and melt, and a decrease in the proportion of plagioclase and quartz for the same temperature range. Although melting began at temperature <800° C, opx did not appear as a stable phase until > 925° C, where its appearance was reversed in both KAL and PON. The only ferromagnesian phases stable until the appearance of opx in both starting materials are biotite, garnet and melt. The abundance of ilmenite increased relative to the starting material in all 7 kbar experiments.

Table 3. Experimental conditions and mineral assemblage.

Run No.	P (kbar)	T (°C)	Duration (hours)	Mineral Assemblage
Ponmudi				
RJ-05	7	800	504	Bio, Grt, Plg, Kfs, Qtz, Ilm, Py, M
RJ-03	7	850	336	Bio, Grt, Plg, Kfs, Qtz, Ilm, M
RJ-33	7	875	336	Bio, Grt, Plg, Kfs, Qtz, Ilm, M
RJ-11	7	900	336	Bio, Grt, Plg, Kfs, Qtz, Ilm, M
RJ-09	7	950	168	Bio, Grt, Opx, Plg, Kfs, Qtz, Ilm, M
RJ-25	7	1000	48	(Bio), Grt, Opx, Plg, Kfs, Qtz, Ilm, M
RJ-27	7	1000	48	
	→7	→925	168	Bio, Grt, Plg, Kfs, Qtz, Ilm, M
RJ-17	10	875	336	Bio, Grt, Plg, Kfs, Qtz, Ilm, Py, M
RJ-15	10	900	336	Bio, Grt, Plg, Kfs, Qtz, Ilm, Py, Ru, M
RJ-13	10	950	168	Bio, Grt, Plg, Kfs, Qtz, Ilm, Ru, M
RJ-23	10	1000	168	Bio, Grt, Plg, Kfs, Qtz, Ilm, M
RJ-31	10	1050	48	Grt, Plg, Opx, Kfs, Qtz, Ilm, Ru, M
RJ-35	10	1050	48	
	→10	→1025	48	Bio, Grt, Plg, Kfs, Qtz, Ilm, M

contd...

Run No.	P (kbar)	T (°C)	Duration (hours)	Mineral Assemblage
RJ-39	12.5	1035	72	Grt, Kfs, Plg, Qtz, Opx, Ilm, M
RJ-19	15	950	240	Bio, Grt, Plg, Kfs, Qtz, Ilm, Ru, Py, M
RJ-21	15	1000	96	Bio, Grt, Plg, Opx, Kfs, Qtz, Ru, M
RJ-29	15	1050	48	Grt, Plg, Kfs, Qtz, Ru, M
RJ-37	15	1050	48	
	→15	→975	72	Bio, Grt, Plg, Kfs, Qtz, Ilm, M
Kalanjur				
RJ-06	7	800	504	Bio, Grt, Plg, Kfs, Qtz, Ilm, Py, M
RJ-04	7	850	336	Bio, Grt, Plg, Kfs, Qtz, Ilm, Py, M
RJ-34	7	875	336	Bio, Grt, Plg, Kfs, Qtz, Ilm, M
RJ-12	7	900	336	Bio, Grt, Plg, Kfs, Qtz, Ilm, M
RJ-10	7	950	168	Bio, Grt, Opx, Plg, Kfs, Qtz, Ilm, M
RJ-26	7	1000	48	(Bio), Grt, Opx, Plg, Kfs, Qtz, Ilm, M
RJ-28	7	1000	48	
	→7	→925	168	Bio, Grt, Plg, Kfs, Qtz, Ilm, M

Run No.	P (kbar)	T (°C)	Duration (hours)	Mineral Assemblage
RJ-18	10	875	336	Bio, Grt, Plg, Kfs, Qtz, Ru, M
RJ-16	10	900	336	Bio, Grt, Plg, Kfs, Qtz, Ilm, M
RJ-14	10	950	168	Bio, Grt, Plg, Kfs, Qtz, Ilm, M
RJ-24	10	1000	168	Bio, Grt, Plg, Kfs, Qtz, Ilm, M
RJ-32	10	1050	48	(Bio), Grt, Opx, Plg, Kfs, Ru, M
RJ-36	10	1050	48	
	→10	→1025	48	Bio, Grt, Plg, Kfs, Qtz, Ilm, M
RJ-40	12.5	1035	72	Grt, kfs, Plg, Qtz, Opx, Ilm, M
RJ-20	15	950	240	Bio, Grt, Plg, Kfs, Qtz, Ru, M
RJ-22	15	1000	96	Bio, Grt, Plg, Kfs, Qtz, Ru, M
RJ-30	15	1050	48	Grt, Plg, Kfs, Qtz, Ilm, M
RJ-38	15	1050	48	
	→15	→975	72	Bio, Grt, Plg, Kfs, Qtz, Ru, M

Abbreviations: Bio – biotite, Grt – garnet, Plg – plagioclase, Kfs – Alkali-feldspar, Opx – orthopyroxene, Ilm – ilmenite, Ru – rutile, Py – pyrrhotite, M – quenched melt. Phase in parentheses indicate that only trace amount of this phase were present. → indicate second-step of the experiment.

10 kbar

Melting occurred in all the runs conducted at 10 kbar in both KAL and PON. The abundance of biotite at any temperature is higher than that in the corresponding low-pressure experiment. However, plagioclase is less abundant and garnet more abundant compared to the low-pressure experiments. The presence of opx was reversed between 1025 and 1050° C. In the single step experiments, opx was observed only at 1050°C, where it occurs as needles and prisms pseudomorphing biotite. Disappearance of opx in the reversal experiment corresponds with the growth of euhedral grains of biotite, as was observed in the reversal experiment at 7 kbar. In addition to ilmenite, rutile is present in some 10 kbar experiments.

12.5 kbar

A single experiment at 1035° C contained garnet as the dominant mafic product phase with subordinate amounts of opx in both samples. Opx occurs as small prismatic crystals in PON in textural contact with newly formed euhedral garnets. In KAL opx also forms large crystals pseudomorphing biotite. Biotite was absent in both samples. The proportion of the melt is greater than the 1000° C run at 7 kbar in both samples. Plagioclase abundance is considerably less than that in the 7 kbar experiments. Ilmenite was the only oxide phase present.

15 kbar

At 950° C, the more friable nature of the run product compared to the corresponding 7 kbar experiment suggests that the proportion of melt is considerably less at 15 kbar. The melt proportion, however, increases substantially from 950° C to 1050° C. Garnet is more abundant than in any of the low-pressure experiments. Garnet grains exhibit zoning in all of the high pressure runs, but the zoning is limited to the outer ~1-1.5 μm of the grains. In the 1050° C experiments the garnet crystals pseudomorph biotite. The proportion of plagioclase has considerably decreased compared to the low-pressure experiments. Opx was observed as a product in the 1000° C run with PON, but is absent from all the other experiments with PON, and from all experiments on KAL at 15 kbar. Biotite was absent from both KAL and PON samples at 1050° C. In a two-step experiment involving equilibration at 1050° C for two days and subsequent equilibration at 975° C for three days, opx was not observed as a phase in both KAL and PON. However, the run product showed growth of biotite as euhedral grains.

Phase compositions

Biotite

Biotite is present as a restite phase in experiments at 1000° C and below but is absent from all higher temperature (>1000° C) experiments except for the run RJ-31 (1050° C, 10 kbar), which contains a few residual grains of the mineral. Biotite typically occurs as elongate (5-50 μm) ribbon-like

grains with resorbed margins (Fig 3A). In most run products, a thin film of quenched melt surrounds the biotite grains. Small (<2 μm) grains of ilmenite and/or rutile commonly nucleate on or near biotite grains.

Biotite compositions are given in Appendix 3. Some biotite analyses showed high silica content due to contamination from the surrounding melt. These analyses (containing > 39 wt. % silica) were discarded and the rest were averaged for each run product. Biotite compositions vary with pressure and temperature in experiments with both PON and KAL. The most notable variations are overall increases in Mg-number, Ti and F of biotite with increasing temperature. I attribute the increase in the Mg-number at temperatures above 875° C (Fig. 4A) to preferential breakdown of the siderophyllite (Fe-Al) component in biotite to produce garnet according to the continuous reaction:

$$\text{Bio} + \text{Plag} + \text{Qtz} = \text{Grt} + \text{Kfs} + \text{Melt}$$
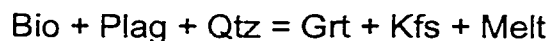
Progress of this reaction from left to right results in a residual biotite with higher Mg and lower Al than the starting biotite. This is evident from Fig. 4B, which shows that there is a general trend towards decreasing Al content with increasing Mg-number. Opx joins the product assemblage at higher temperature but has the same general effect on the Mg-number of the residual biotite.
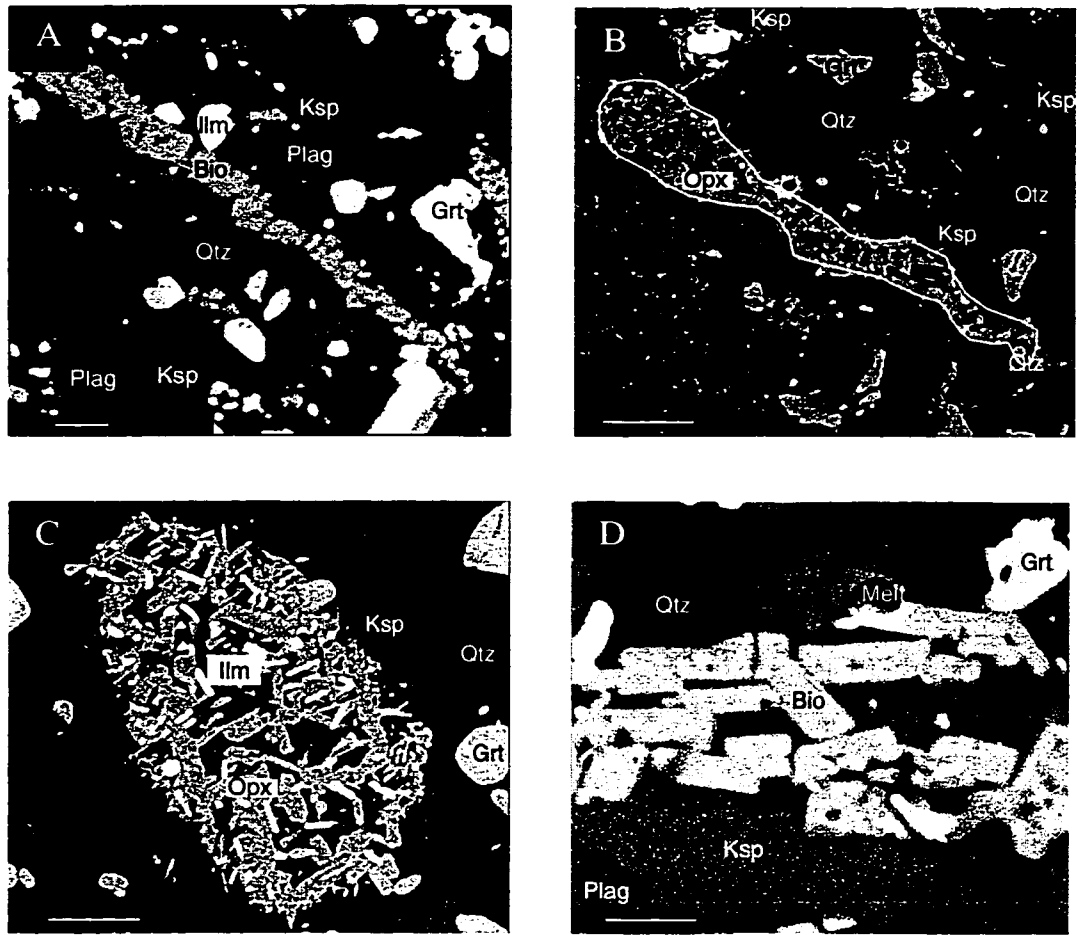
Figure 3. Backscatter electron images of run products. **A.** Typical morphology of biotite in single-step experiments in which melting occurred. Note the highly resorbed margins indicative of its break down. **B.** Matted orthopyroxene crystals pseudomorphing biotite in the 7 kbar, 1000° C experiment on Ponmudi. **C.** Prismatic crystals of orthopyroxene that grew in the 7 kbar, 1000° C experiment on Kalanjur. Also note the tiny needles of ilmenite. **D.** Euhedral biotite crystals that grew in the reversal experiment at 7 kbar on Ponmudi. The euhedral biotite growth and the absence of orthopyroxene in these runs were used as criteria for a successful reversal of opx-in reaction. Scale bar in each image is 5 m.

24
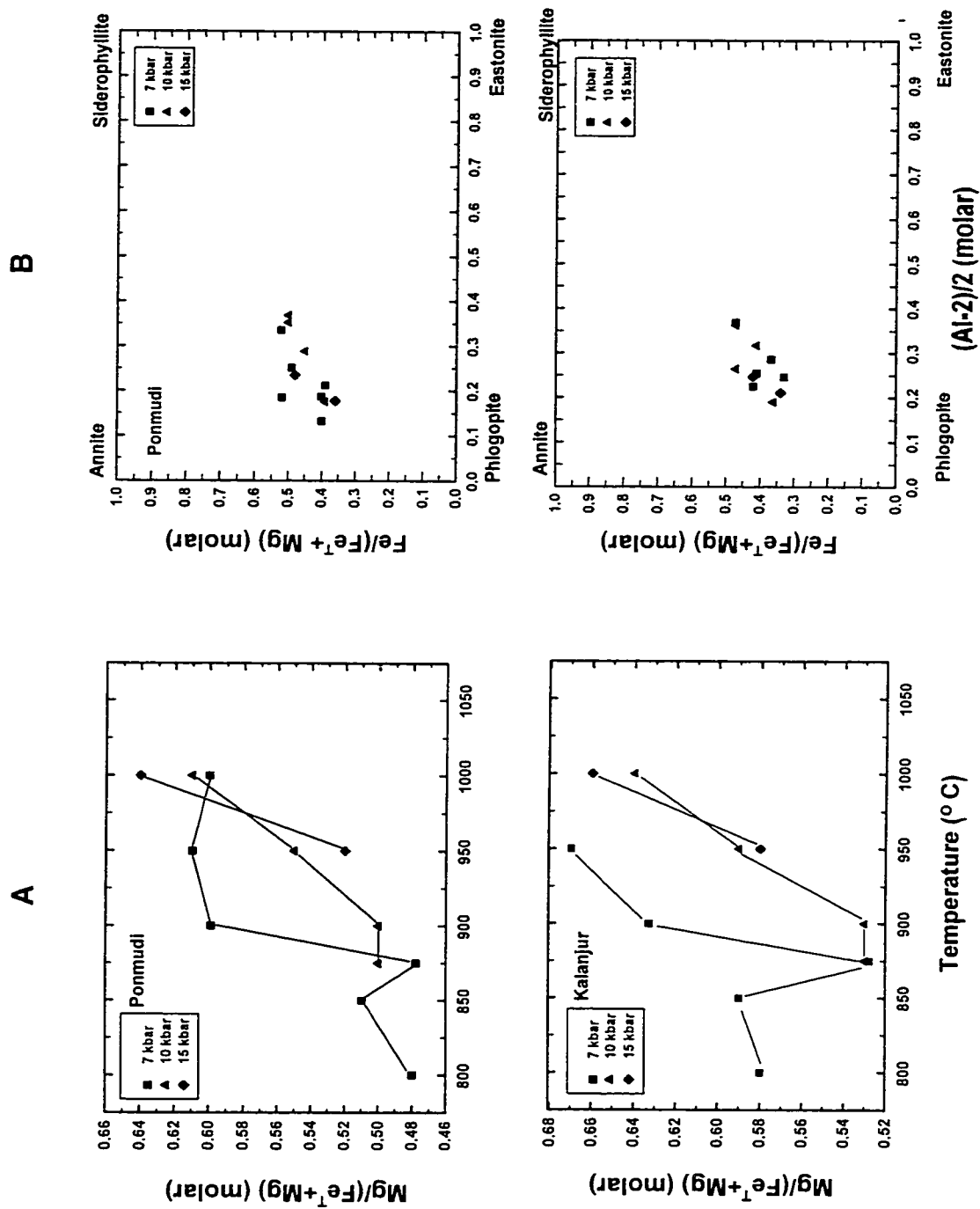
Figure 4. Biotite compositions. A. molar Mg/(Mg + Fe^T) vs. temperature. B. Annite - Eastonite diagram illustrating the variation of Al content with Fe/Mg ratio.

The increase in the F content of biotite (Fig. 5) with the progress of fluid-absent melting is consistent with the similar trend observed in previous studies (Peterson et al., 1991; Patiño Douce and Beard, 1995; Pickering and Johnston, 1998). F substitution is enhanced by the fact that biotite becomes progressively more Mg-rich with increasing temperature. Thus, because of the crystallo-chemical Fe-F avoidance (or Mg-F affinity) effect (Rosenberg and Foit, 1977), F substitutes more readily into Mg-rich biotite.

The increase in the Ti content of biotite at temperatures above 875° C (Fig. 5) is also consistent with the observations made in previous studies (Patiño Douce and Beard, 1995; 1996; Pickering and Johnston, 1998). Several mechanisms have been proposed for Ti substitution in biotite. These include Ti-oxy ($TiO^{2-}{}_2R^{2+}{}_{-1}OH^-{}_{-2}$), Ti-Tschermak's ($TiAl_2R^{2+}{}_{-1}Si_{-2}$), and Ti-vacancy ($Ti\square R^{2+}{}_{-1}$) substitution mechanisms, where R represents a divalent cation such as Fe^{2+} or Mg^{2+} (Bohlen et al., 1980; Abrecht and Hewitt, 1988; Dooley and Patiño Douce, 1996). The Ti-oxy substitution mechanism results in the formation of a progressively dehydroxylated biotite. This mechanism may be significant in the present experiments but is difficult to evaluate rigorously without direct determination of the water content of biotite in run products. The Ti-Tschermak's substitution can be ruled out because it predicts a positive correlation between Ti and Al rather than the crude negative correlation observed in the present experiments (Fig. 6). Similarly, two lines of evidence suggest that the Ti-vacancy mechanism was not a
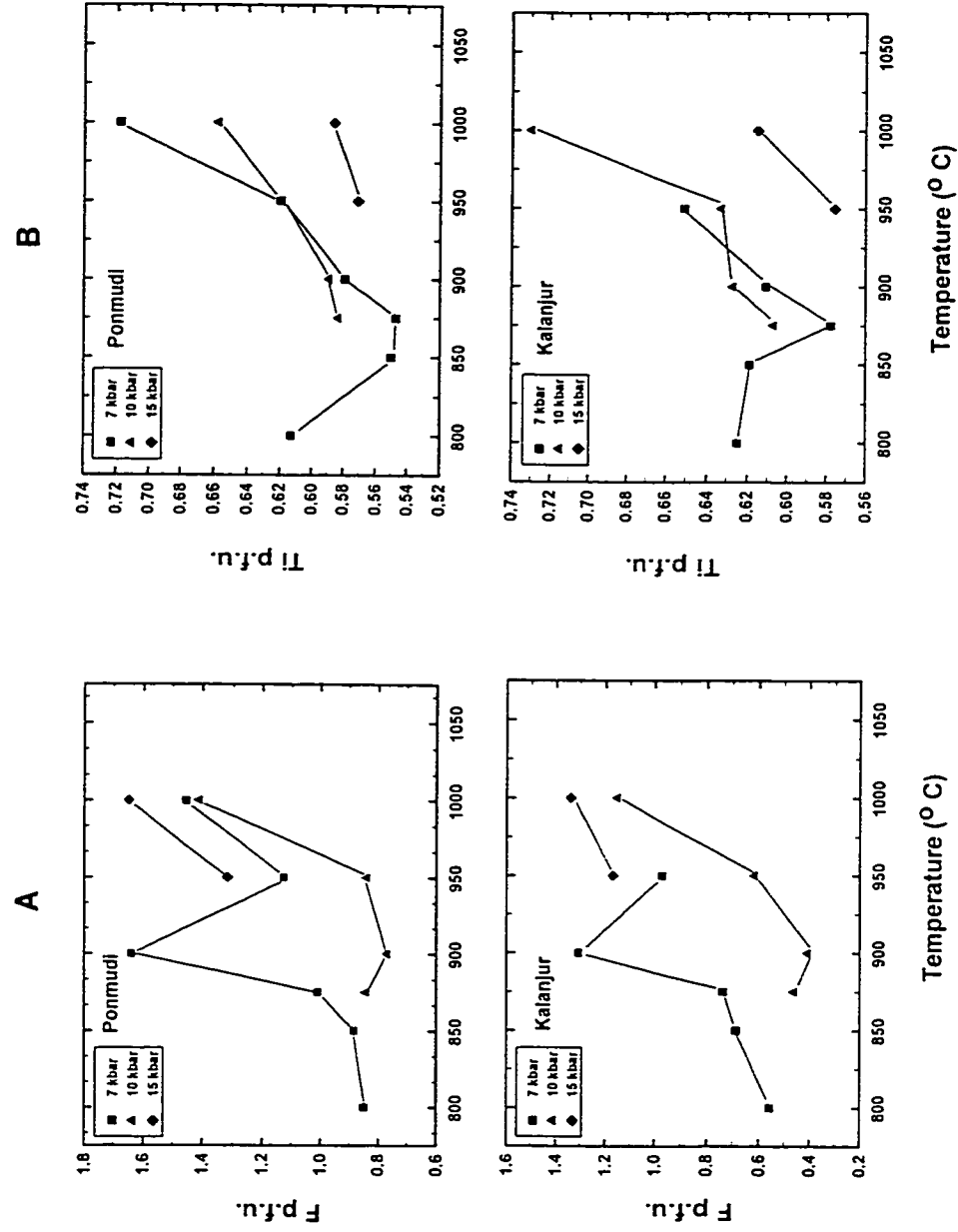
Figure 5. Biotite compositions. A. F p.f.u. vs. temperature. B. Ti p.f.u. vs. temperature.

27
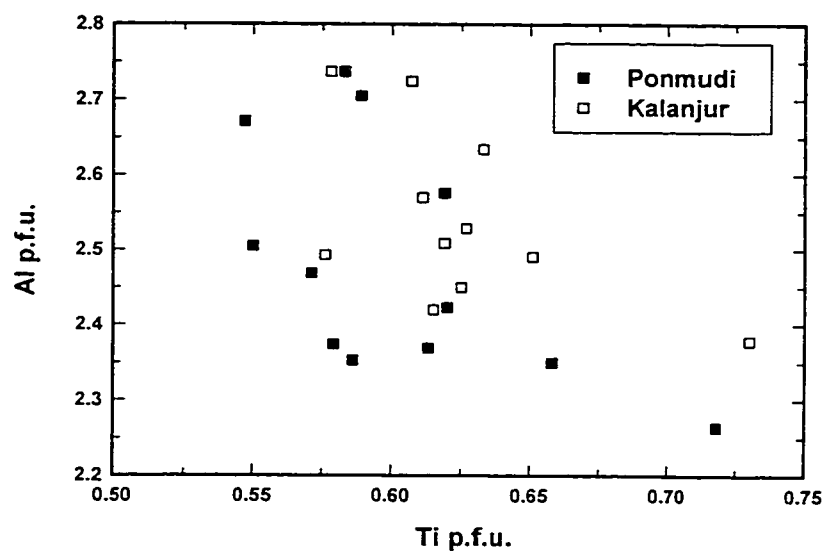
Figure 6. Variation of molar Al with Ti in biotite.

Figure 7. Crystal-chemical effects of Ti substitution in biotite. A. Octahedral vacancy vs. Ti B. (Ti + Oct. Al/2)-octahedral vacancy vs. (Ti + Oct. Al/2).

29
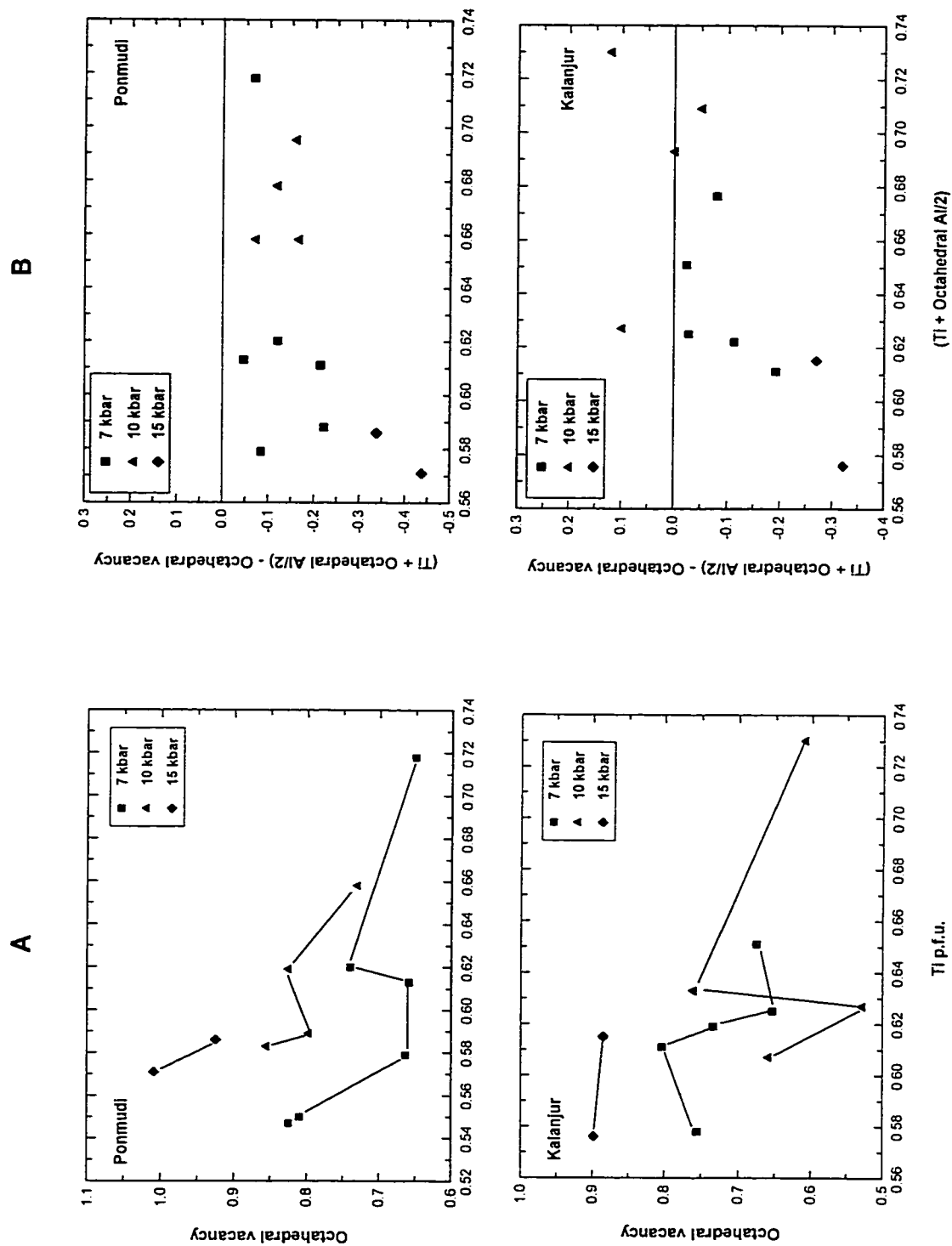
dominant substitution mechanism in my experiments. Firstly, there is a negative correlation between Ti and the number of octahedral vacancies, rather than the positive correlation expected with this substitution (Fig. 7A). Secondly, in almost all analyzed biotites, the total number of octahedral vacancies exceeds that required to charge balance Ti and Al substitution in the octahedral sites (Fig. 7B). This implies the presence of an additional high valency cation, most likely Fe^{3+}. The excess vacancies can be accounted for if approximately 7 to 30 % of the total iron in the experimental biotite are ferric rather than ferrous. This amount of ferric iron is broadly consistent with the measured Fe^{3+} contents of metamorphic biotite (Guidotti and Dyar, 1991). A possible mechanism to account for Ti substitution and the observed negative correlation between Ti content and octahedral vacancies is a Ti-ferric iron substitution ($Ti^{4+}_2 R^{2+}_5 Fe^{3+}_{-6} \square_{-1}$). This mechanism increases octahedral site occupancy by replacement of Fe^{3+} and octahedral vacancies by Ti and divalent cations. Detailed evaluation of the proposed substitution mechanism requires data on the Fe^{2+}/Fe^{3+} ratios of starting and run product biotites.

The effect of pressure on biotite composition is less clear but, in general, increasing pressure at constant temperature decreases the Ti content and Mg-number of the biotite.

Garnet

Garnet is both a relict and a neoblastic phase in all the experiments. Newly grown garnet mostly nucleated as discrete grains, although growth also occurred on the rims of pre-existing garnet grains. Garnet neoblasts can be distinguished from relict grains by their euhedral shape and the presence, in some cases, of melt inclusions. The neoblasts commonly formed in the vicinity of relict biotite crystals with textures suggestive of formation through biotite breakdown. The abundance of garnet increases with pressure, with the largest increase between 10 and 15 kbar.

Garnet grains range in size from <1 to >15 μm. The composition of larger grains varies only slightly with changing pressure and temperature, suggesting that these grains did not equilibrate compositionally during the experiments. Smaller euhedral grains, however, do show compositional variation with changing pressure and temperature. The compositions given in Appendix 4 are an average of analyses on small euhedral crystals and on rims of larger grains where such analyses were possible.

The composition of neoblastic garnet is remarkably uniform in each run product. Garnet in both PON and KAL are dominantly almandine-pyrope solid solutions and generally contain less than 10 mol % grossular component. The grossular component of garnet in PON is, however, systematically higher than that of KAL, reflecting differences in the bulk composition of the two starting materials.

The Mg-number of garnet increases with temperature at constant pressure (Fig. 8A). This effect is more pronounced in the 10 and 15 kbar experiments with PON. In the experiments with KAL, this trend is discernible only at 10 kbar. The grossular content of garnet marginally increases with temperature in KAL (Fig. 8B). In PON, however, the trend is observable only at 15 kbar. The compositional variation in garnet with pressure is less distinct but show an overall trend towards increasing Mg-number and grossular content with increasing pressure at constant temperature.

Plagioclase

Plagioclase is a common restitic phase in all the run products and ranges from < 1 μm to more than 15 μm in diameter. It mostly occurs as anhedral grains and decreases in abundance with increasing temperature suggesting that it is a reactant phase in the melting reactions. Attainment of equilibrium composition in plagioclase grains is considered to be a problem in fluid-absent melting experiments with granitic rocks (Johannes, 1984). The composition of the plagioclase crystals (Appendix 5) in the present study, however, are different from the starting plagioclase suggesting their reactivity during the experiments. The plagioclase is also uniform in composition on an intra-grain as well as on intra-sample scale. Montel and Vielzeuf (1997) reported excess silica and/or Al in their plagioclase grains, but no indication of this non-stoichiometry was noted in the plagioclase analyses of the present study.
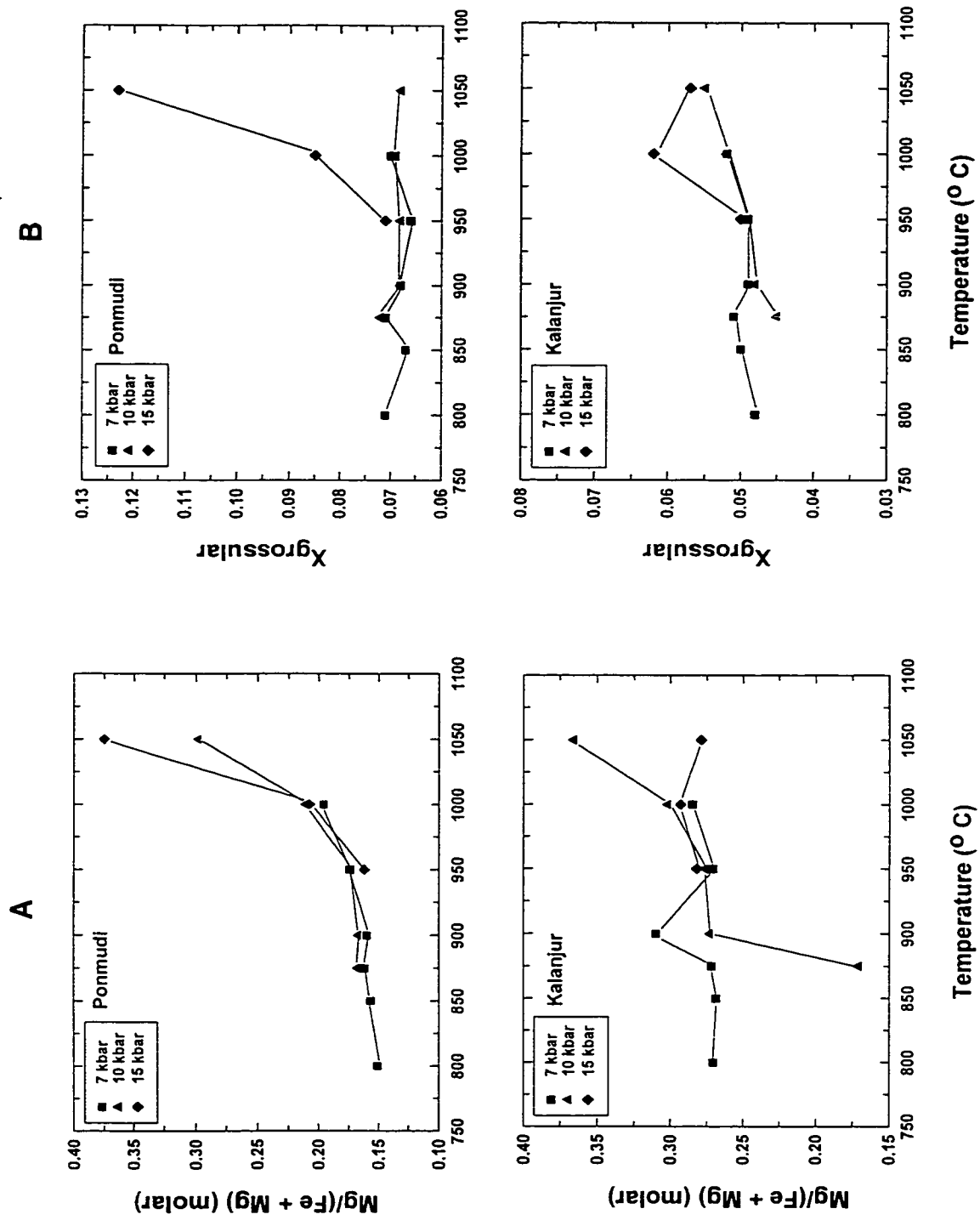
Figure 8. Garnet compositions. **A.** molar Mg/Fe + Mg vs. temperature. **B.** $X_{grossular}$ vs. temperature.
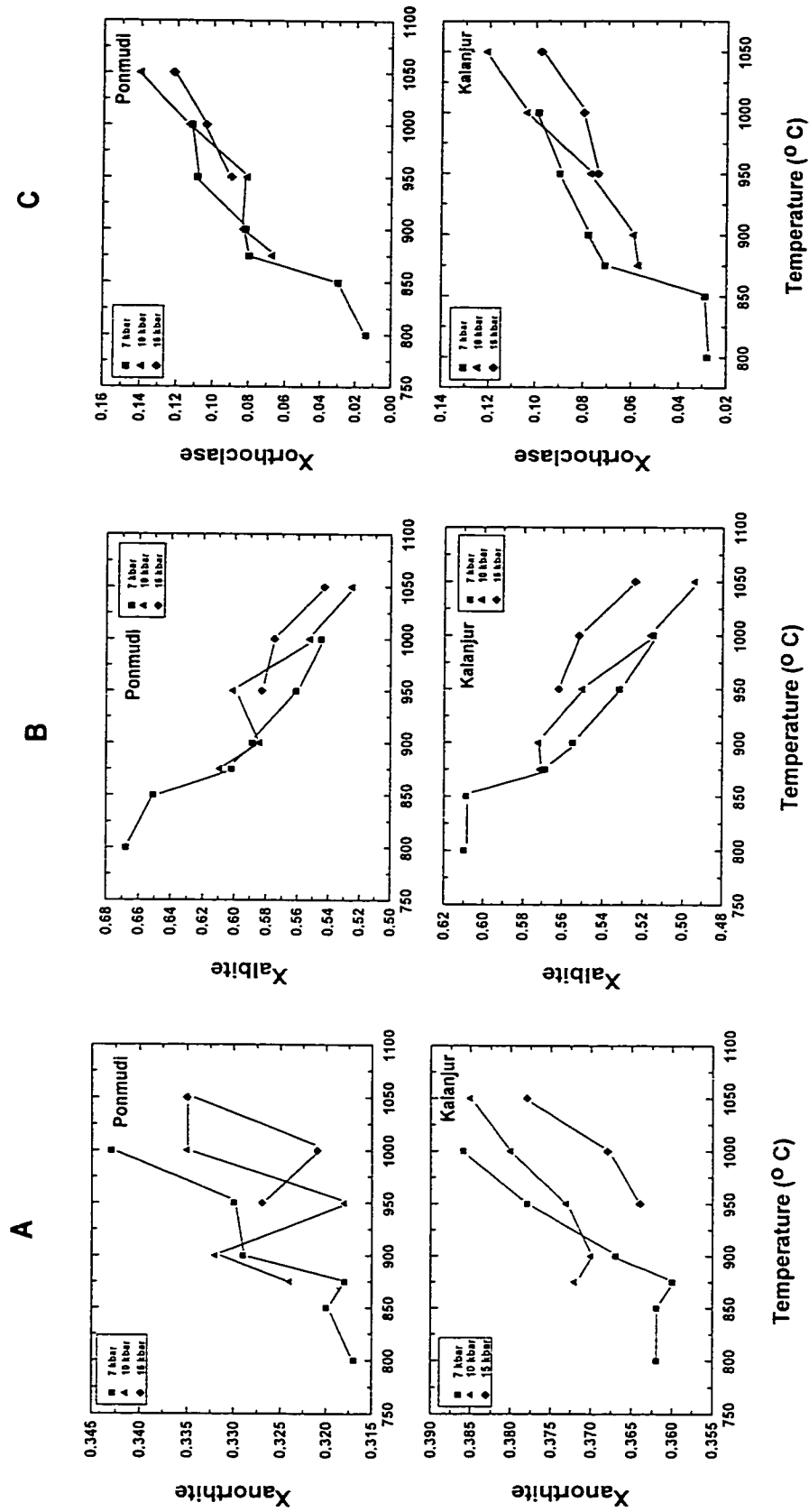
Figure 9. Plagioclase compositions. A. $X_{anorthite}$ vs. temperature. B. X_{albite} vs. temperature. C. $X_{orthoclase}$ vs. temperature.

34

There is consistent compositional variation in the plagioclase grains with temperature and pressure. At constant pressure, the anorthite content increases with increasing temperature (Fig. 9A). This reflects the preferential incorporation of the albite component of plagioclase into the melt leaving behind a more anorthitic plagioclase. There is also a consistent increase in the orthoclase content of plagioclase with temperature (Fig. 9), which is a consequence of the shrinkage of the ternary feldspar solvus with increasing temperature. The plagioclase compositions generally plot within 50° C of the appropriate isotherm on the ternary feldspar solvus (Elkins and Grove, 1990).

Changes in plagioclase composition with increasing pressure are subtler but, in general, the anorthite content of the plagioclase decreases with increasing pressure (at constant temperature). This trend is most clearly seen in the KAL experiments at temperatures of 950° C and above (Fig. 9), and can be attributed to breakdown of anorthite component of plagioclase to form grossular component in garnet. There are also small decreases in the orthoclase content of plagioclase with increasing pressure, which is consistent with expansion of the ternary feldspar solvus with pressure (Elkins and Grove, 1990).

Alkali-Feldspar

Alkali feldspar is a common neoblastic phase in all experiments that produced melt. It occurs as homogenous crystals, up to 10 μm in diameter,

and commonly in contact with restitic plagioclase grains. Some of the alkali-feldspar grains that are larger than 10 μm could be relict. However, no compositional differences were observed between these and the smaller crystals suggesting that all grains were compositionally equilibrated.

In contrast to the present experiments, alkali feldspar was not observed as a product of biotite fluid-absent melting in many previous studies (Vielzeuf and Holloway, 1988; Patiño Douce and Johnston, 1991; Vielzeuf and Montel, 1994; Patiño Douce and Beard, 1996). Patiño Douce and Beard (1995;1996) attributed the absence of alkali feldspar in their run products to nucleation difficulties arising from limited temperature range of coexistence of this phase and melt. Carrington and Watt (1995) proposed that the behavior of alkali feldspar during fluid-absent melting depends upon the relative H_2O/K_2O ratio of melt and biotite, and that higher H_2O/K_2O ratio in melt favors production of alkali feldspar during melting. The absence of alkali feldspar in some of the earlier studies could be attributed to the fact that it was not present in the starting material of those experiments. Therefore, any alkali feldspar produced by biotite breakdown was incorporated as orthoclase component in plagioclase or melt (Vielzeuf and Montel, 1994). In contrast, the presence of 10 – 15 modal percent of alkali feldspar in the starting materials of the present experiments allowed neoblastic alkali feldspar to be preserved.

Alkali feldspar compositions vary consistently with temperature (Appendix 6 and Fig. 10). The orthoclase content decreases whereas the anorthite and albite content increases with increasing temperature. This can

36
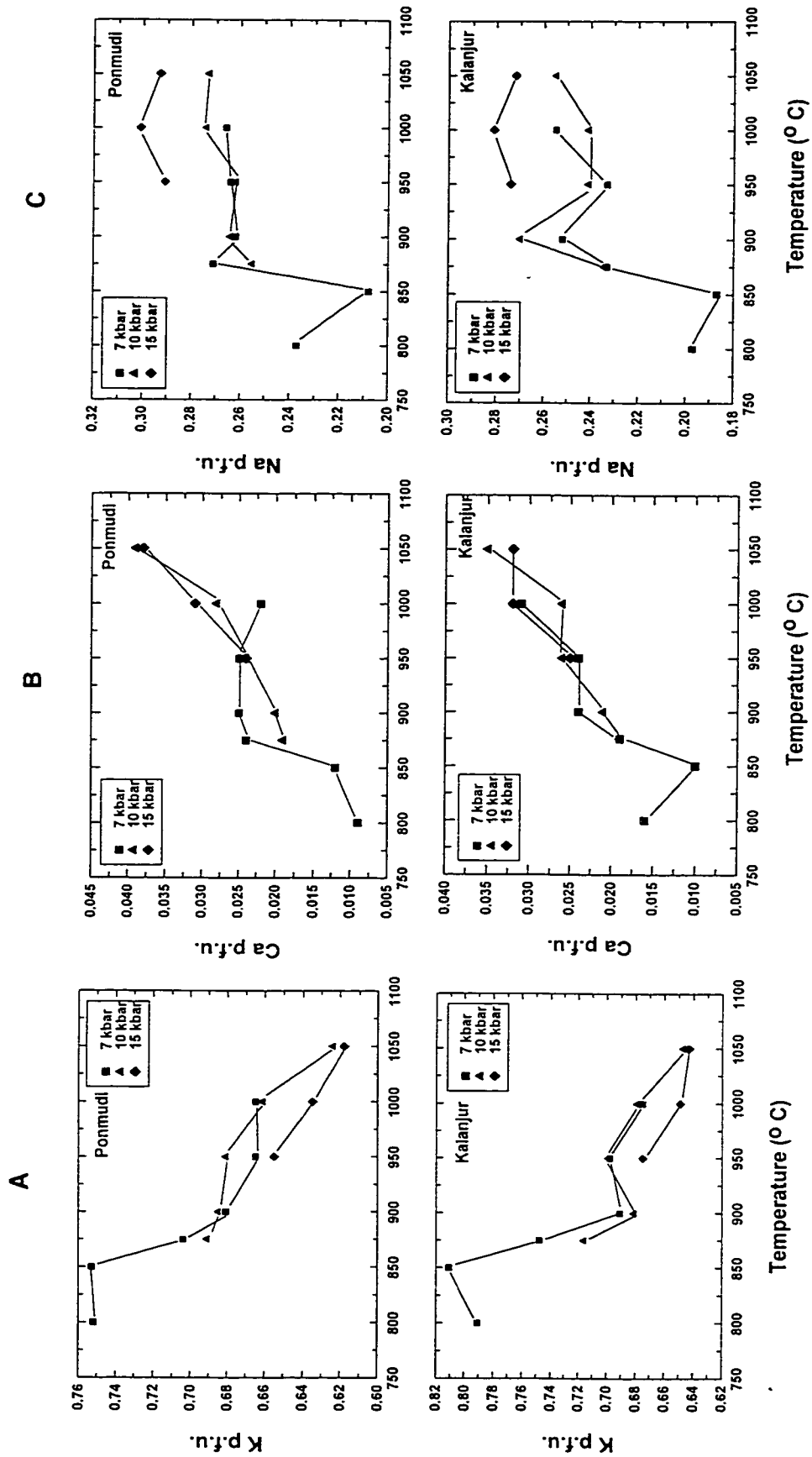
Figure 10. Alkali-feldspar compositions. A. K p.f.u. vs. temperature. B. Ca p.f.u. vs. temperature. C. Na p.f.u. vs. temperature.

37

be attributed to the increased solubility of plagioclase component in alkali feldspar with increasing temperature.

Orthopyroxene

Opx was a product of biotite fluid-absent melting in the experiments at temperatures above $925°$ C and at $1050°$ C in both starting materials at 7 and 10 kbar, respectively. It was also observed in the run product of $1000°$ C experiment with PON at 15 kbar. In these experimental products opx has a characteristic prismatic to needle-like habit and commonly occurs as grains pseudomorphing biotite (see Fig. 3). The width of the opx crystals was usually less than 1 μm making quantitative elemental analyses difficult. Opx analyses was performed with a focussed beam to minimize contamination from surrounding grains. Nevertheless, the resulting analyses (see Appendix 7 for average) still incorporated small amounts of surrounding ilmenite, and/or melt as is evident from their higher TiO_2 and K_2O content. The analyses were corrected assuming all K in opx represents contamination from quenched melt (glass).

The opx are characterized by high Al_2O_3-content (6.8 – 7.9 wt. % and 5.1 – 9.8 wt. % in PON and KAL, respectively), consistent with the high temperatures of their formation. The Al_2O_3 content increases with temperature at constant pressure. Although the variation of Mg-number of the orthopyroxenes with temperature is unclear due to the fewer data available,

38

the Mg-number of opx grains were greater than those of the coexisting biotite grains. The opx in KAL is generally more magnesian than in PON, reflecting the more magnesian nature of the KAL starting material.

Fe-Ti oxides

Ilmenite is the dominant Fe-Ti oxide mineral in most of the run products. At pressures $\geq$ 10 kbar, it is accompanied by rutile. The hematite component of ilmenite is low and varies from ~3 to 7 mol % in both KAL and PON (Appendix 8). Rutile grains were not analyzed quantitatively.

Melt

Glass (quenched melt) is present in all the run products. It occurs mostly as thin films around biotite and garnet and also as isolated pockets. The melt pockets were too small to get reliable analyses in most cases. The available data indicates that the melts are peraluminous and remain leucocratic to high temperatures (Appendix 9). The proportion of melt increases with temperature but remains nearly constant with increasing pressure.

Discussion

Approach to equilibrium

Demonstration of the attainment of equilibrium during the experiments is important for unambiguous interpretation of the results. The following criteria were considered in assessing the approach to equilibrium conditions in the current experiments:

1. *Phase reversals.* The most rigorous evidence for attainment of equilibrium is provided by successful phase reversals. The first appearance of opx was reversed at 7 and 10 kbar in both starting materials. To my knowledge, these are the first successful reversals of a fluid-absent melting reaction in experiments with natural samples.

2. *Homogeneity of phases.* Most of the phases observed in the run products were compositionally homogenous, suggesting an approach to equilibrium. Garnet was the only phase that showed significant heterogeneity in composition within a single run product. The larger garnet crystals were compositionally similar to the starting garnet whereas the smaller euhedral garnets were closer to being in equilibrium at experimental P-T conditions. Compositional equilibration in garnet was also found to be a problem in many previous fluid-absent melting experiments (e.g., Le Breton and Thompson, 1988; Carrington and Harley, 1995). Nevertheless, changes in garnet composition in the higher temperature and/or pressure experiments suggest that the phase was at least reactive during the experiments.

3.	*Systematic variation in phase proportions and compositions.* The abundance of phases changed in a consistent manner with temperature and pressure. Most notable among these changes was the decrease in the abundance of biotite and plagioclase with increasing temperature, the increase in abundance of garnet with temperature and pressure, and the appearance and increase in abundance of opx with temperature in the 7 kbar experiments. Phases generally also showed consistent variation in composition with temperature and pressure, with the clearest compositional trends noted in plagioclase, alkali-feldspar and biotite. With the exception of garnet, all the phases present in the run products had a different composition than that of the starting material.

4.	*Reproducibility.* The utilization of two starting materials with similar bulk compositions provide an independent check on the degree of equilibration as stabilization of widely different assemblages in the two starting materials at the same P-T conditions would suggest a lack of equilibration in one or both sets of experiments. In the present study, the two starting materials produced similar mineral assemblages when subjected to the same experimental conditions. Moreover, the phase compositions in both the samples showed similar variation with changing P-T conditions.

The above observations suggest that the present experiments were of sufficiently long duration to achieve phase equilibrium, and show a reasonable approach to compositional equilibrium for most phases. Accordingly, the interpretations that follow assume that the phase assemblages and

compositions observed in the experimental run products approximate those that would be present in nature at similar P-T conditions.

Melting reactions

My results represent the phase relations in natural high-grade semi-pelitic rocks in the P-T range where they undergo amphibolite- to granulite-facies transition. In peraluminous quartzofeldspathic rocks, this P-T region corresponds to the conditions where muscovite has already disappeared from the rocks through prograde metamorphic reactions, leaving biotite as the only significant reservoir of volatiles in the amphibolite-granulite transition zone. The following melting reactions were identified in the present experiments, based mainly on textural relations and variation in the phase assemblages with pressure and temperature.

Fluid-absent solidus

As the focus of the present study was not to constrain the beginning of melting in quartzo-feldspathic rocks, the position of fluid-absent solidus was not bracketed in P-T space. Nevertheless, textural relations between phases as well as the observed variation in the proportion and composition of different phases provide a reasonable indication of its P-T position. Quenched melt was observed in all 7 kbar run products. However, only trace amounts of melt (<5 %) were identified in the runs up to a temperature of 900° C in both starting materials. I interpret the quenched melt observed at temperatures

<875° C to be the result of fluid-present melting. Despite the extreme care taken to eliminate moisture during sample preparation and loading, the hygroscopic nature of the finely powdered starting materials invariably results in the adsorption of some H_2O. At experimental temperatures, which in this study exceeded the H_2O-saturated solidus by 150° C or more, the presence of even small amounts of moisture (0.5 wt. %) would result in non-negligible amounts of vapor-saturated melting. I suggest, therefore, that the trace amounts of melt present in lower temperature experiments was produced by this process and that fluid-absent melting (by biotite breakdown) only began at temperatures > 875° C. This interpretation is supported by the absence of significant compositional variation in biotite until temperatures ≥ 875° C. Therefore, 875° C is assumed as the fluid-absent solidus for PON and KAL at 7 kbar. At 10 kbar, phase compositional variations are generally more pronounced above 900° C which is therefore inferred to be the position of fluid-absent solidus at this pressure.

The phase relations are consistent with a fluid-absent solidus reaction of the type:

Biotite + Plagioclase + Quartz = Garnet + K-feldspar + Melt------------- (1)

This is interpreted from an increase in modal abundance of garnet and alkali-feldspar concomitant with a decrease in biotite and plagioclase proportions in experiments at temperatures exceeding the fluid-absent solidus.

Orthopyroxene-in reaction

The second reaction, which was the principal focus of the present study, corresponds to the first appearance of opx (Fig. 11). Based on the decrease of biotite and plagioclase concomitant with the appearance and increase of opx and garnet with increasing temperature, I interpret the opx-forming reaction to be:

Biotite + Plagioclase + Quartz =

Orthopyroxene + Garnet + K-feldspar + Melt--(2)

The reaction has a relatively shallow positive slope between 7 and 10 kbar but steepens above 10 kbar and may in fact bend back at higher pressure to a negative dP/dT slope. The back bending of reaction (2) was documented in PON in which opx was observed in the run product at 1035 and 1000° C at 12.5 and 15 kbar, respectively. In KAL, however, opx was not observed at 15 kbar. Nevertheless, the occurrence of opx in the 1035° C, 12.5 kbar experiment confirms a steepening of the reaction curve.

I attribute the steepening in the slope of the opx-in curve at high pressures to a significant change in the stoichiometry of the melting reaction, such that the volume change of the reaction changes from positive to negative. This is evident from changes in the modal abundance of reactant
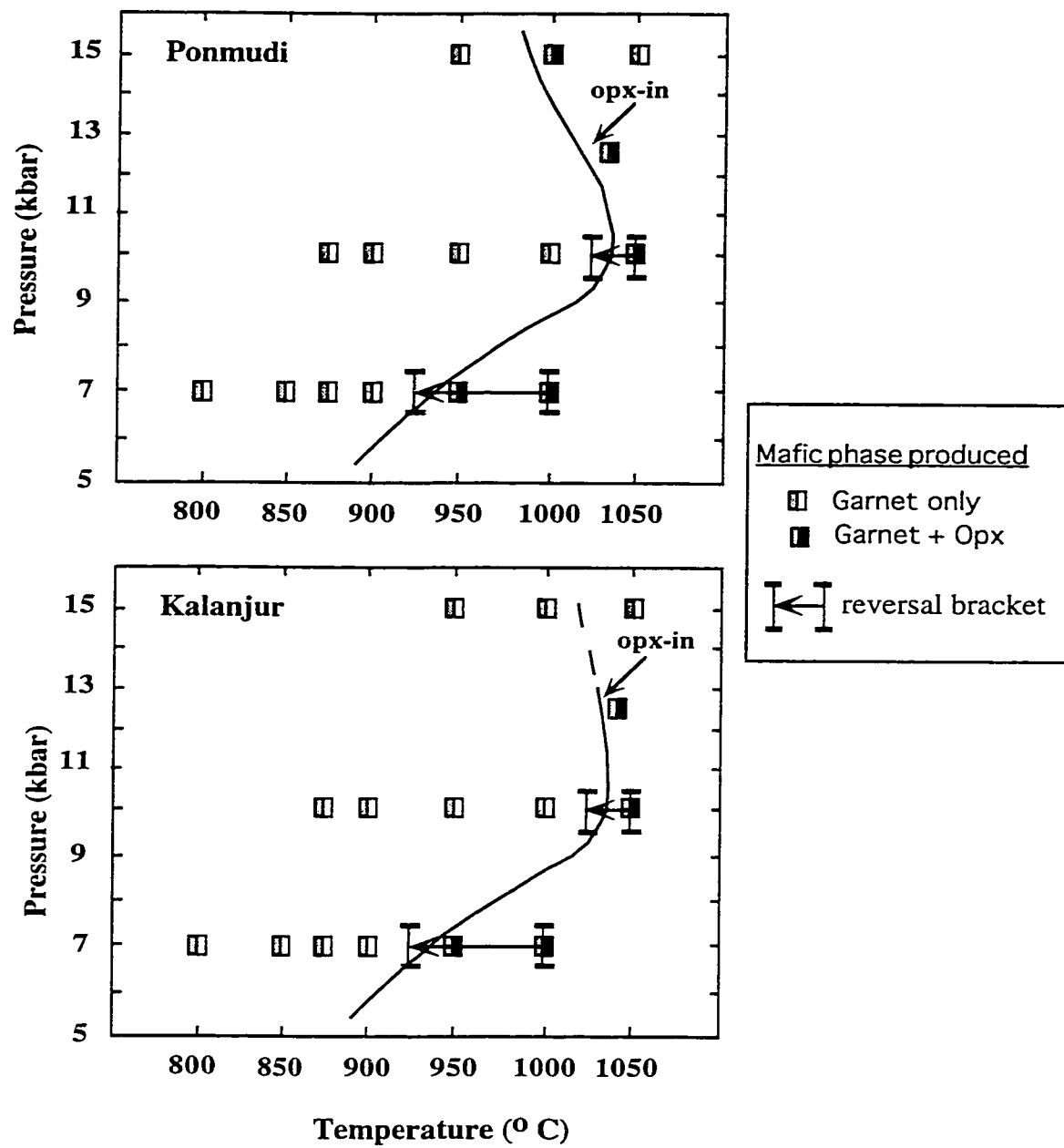
Figure 11. P-T location of the orthoproxene-in curve obtained in the present study.

and product minerals with increasing pressure without significant changes in the proportion of melt produced. With increasing pressure (at constant T), changes include increase in the modal abundance of biotite, garnet and alkali-feldspar, and a decrease in the abundance of plagioclase and opx. The residual plagioclase in the high-pressure experiments is also markedly more albite-rich than in the low-pressure experiments. These observations suggest increased production of garnet through the melting reaction at the expense of plagioclase and opx. Biotite contributes proportionately less to the melting reaction at high pressure.

Comparison with previous studies

The results of this study provides interesting comparisons with the studies of Vielzeuf and Montel (1994), Patiño Douce and Beard (1995, 1996), and Stevens et al. (1997), which also investigated the fluid-absent melting behavior of semi-pelitic bulk compositions (see Table 4 for compositions). The mineralogical and chemical composition of materials used in these other studies was broadly similar to the present experiments. There were, however, some differences, including the presence of K-feldspar and a significantly lower modal proportion of biotite in the starting materials of the present study.

The major difference in the starting materials used in the present study from that of previous studies is in the composition of biotite. As stated previously, the biotite composition in the present starting materials is more representative of biotite in natural amphibolite-granulite transitional terranes,

Table 4. Composition of starting materials in previous semi-pelite melting experiments compared with that of present study.

Study	V & M (1994)	P & B (1995)	P & B (1996)	St et al. (1997)	St et al. (1997)	This study	This study
Sample	CEVP	SBG	SMAG	A	NB	Ponmudi	Kalanjur
Wt. % Ti in biotite	2.8	3.9	4.6	0	2.3	5.0	5.4
Wt. % F in biotite	n	0.3	0.1	n	n	1.3	1.4
X_{Mg} in biotite	0.44	0.55	0.23	0.49	0.58	0.46	0.56
X_{An} in plagioclase	22	38	38	35	35	32	37
Wt. % Al_2O_3 in biotite	19.5	14.4	13.2	16.2	20.2	13.7	13.6
modal % biotite	25	37.2	37.2	39	39	10	11
Whole-rock X_{Mg}	47	52	22	49	58	23	31

V & M (1994) – Vielzeuf and Montel, 1994; P & B (1995) – Patino Douce and Beard, 1995; P & B (1996) – Patino Douce and Beard, 1996; St et al. (1997) – Stevens et al., 1997. X_{Mg} – molar Mg/(Fe + Mg); n – not given; X_{An} – molar- Ca/(Ca + Na + K).

47

particularly with regard to their Ti and F content. Although biotites used by Patiño Douce and Beard (1995, 1996) had a relatively high Ti content, the F content of the biotites were negligible. Additionally, the high-Ti biotite used by Patiño Douce and Beard (1996) was more Fe-rich than those commonly found in transitional terranes. Below, the melting relations derived in this study are compared with those reported in previous fluid-absent melting experiments on semi-pelitic bulk compositions.

Fluid-absent solidus

The fluid-absent solidus reaction (1) inferred in my study is consistent with the observation of Vielzeuf and Montel (1994) that, at pressures > 5 kbar, the beginning of melting does not coincide with the formation of opx but is associated instead with a garnet-producing reaction. In contrast to the present results, however, Vielzeuf and Montel (1994) did not find alkali feldspar as a discrete phase in their experimental products and interpreted the increase in the orthoclase component of the plagioclase to indicate that K-feldspar was a product phase. The phase relations reported by Patino Douce and Beard (1996) at pressures > 10 kbar are also consistent with solidus reaction (1), although they too did not report alkali feldspar in their run products. In the more magnesian bulk compositions studied by Patino Douce and Beard (1995) and Stevens et al. (1997), the fluid-absent solidus coincided with an opx-forming reaction. These differences in phase relations likely reflect the strong control of Fe-Mg ratio on the stability of opx relative to garnet (cf. Patino Douce and Beard, 1996).

48

All of the studies noted above found a steep dP/dT slope for the solidus reaction. This is corroborated by the present study where fluid-absent melting was inferred to begin at 875° C at 7 kbar and between 875 and 900° C at 10 kbar. The major difference in the results of the present study is that the temperature of the fluid-absent solidus is 20 to 90° C higher than reported in earlier studies. I attribute this difference to the higher Ti and F content of biotite in the starting materials used in the present experiments. In contrast to this interpretation, Stevens et al. (1997) argued that Ti substitution in biotite does not affect the temperature of the fluid-absent solidus, although it does extend the temperature range over which biotite undergoes fluid-absent melting. They based this conclusion on the similarity of solidus temperatures obtained with their Ti-bearing and Ti-free starting materials (Table 4). However, comparison of the solidus temperatures reported by Stevens et al. (1997) (~800-835° C) with those of Patino Douce and Beard (1995) (850-875° C) and the present study (875-900° C) suggests that increasing the Ti content of biotites with comparable Mg-number significantly increases the solidus temperature. The apparent absence of a stabilizing effect of Ti in Stevens et al. (1997) experiments may be due to the fact that their high Ti biotite ('NB') was also ~20 % higher in Al than their Ti-free biotite ('A'). As noted previously, compositional trends in the biotites of the present experiments suggest that Al-rich biotite breaks down at lower temperature than Al-poorer biotite. Thus, in the Stevens et al. experiments, the stabilizing effect of Ti in biotite may have been masked by the destabilizing effect of high Al.

Orthopyroxene-in reaction

Vielzeuf and Montel (1994) also suggested reaction (2) as the opx-forming reaction in their study. Their results indicate opx formation at 850 and 890° C at 7 and 10 kbar, respectively. The reaction was not tightly bracketed at pressures above 10 kbar. In the more magnesian bulk composition (SBG) of Patiño Douce and Beard (1995), opx was observed as product phase in all experiments in which melting occurred as well as in some sub-solidus experiments. However, in their experiments, garnet was a stable phase only at pressures above 10 kbar. Assuming their solidus to be the opx-in reaction, the reaction has a positive dP/dT slope. At 7 kbar, opx is the product of melting in their experiments at 875° C and its formation was bracketed between 875 and 900° C at 10 kbar. Patiño Douce and Beard's (1996) experiments in a Fe-rich bulk composition suggest a reaction similar to (2) as the opx-forming reaction. They found opx as a product phase at 850° and 925° C at 7 and 10 kbar, respectively. Stevens et al. (1997) did not provide an opx-in curve in their P-T diagram, although, the phase assemblage in their run products indicates opx formation at temperatures between 850° and 950° C (depending upon the Mg-number of the bulk rock) at 10 kbar.

The P-T location of the orthopyroxene-in (opx-in) reaction determined from the present experiments is compared with the opx-in curves of previous semi-pelite fluid-absent melting experiments in Fig. 12. The appearance of opx in my experiments occurs at temperatures higher than that of previous

50
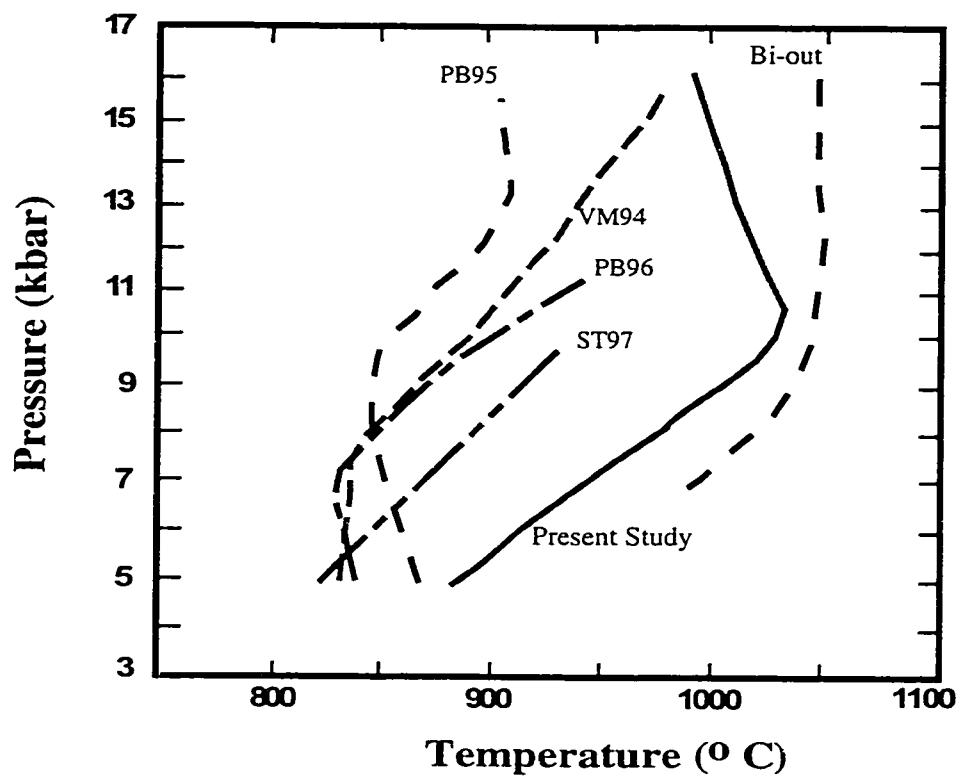
Figure 12. P-T diagram comparing the orthopyroxene-in curve obtained in this study with those from previous fluid-absent melting studies. ST97-Stevens et al. (1997), PB96-Patino Douce and Beard (1996), PB95-Patino Douce and Beard (1995) and VM94-Vielzeuf and Montel (1994).

51

experiments. At 7 kbar, the difference in temperature is about 50° C or greater. At 10 kbar, the difference is more than 100° C. I again attribute the high temperatures required for opx stabilization to the higher Ti and F content of biotites in my study. This result is consistent with the observations made in previous studies that the presence of these elements extends the stability of biotite to higher fluid-absent melting temperatures (Forbes and Flower, 1974; Trønnes et al., 1985; Le Breton and Thompson, 1988; Peterson et al., 1991; Patiño Douce, 1993).

The present study also indicates a positive slope for the opx-in reaction between 7 and 10 kbar, consistent with previous studies. However, the slope of the reaction between 7 and 10 kbar has a much shallower dP/dT slope (~33° C/kbar) than found in by other studies (~10° C/kbar Vielzeuf and Montel (1994), ~3° C/kbar Patiño Douce and Beard (1995), ~25° C/kbar Patiño Douce and Beard (SMAG, 1996). This could also be attributed to the stabilizing effect of Ti and F on biotite, extending the P-T region between the beginning of melting and the appearance of opx with increasing pressure. None of the previous studies have documented a reversal in the slope of the opx-in reaction between 10 and 15 kbar.

Biotite fluid-absent melting interval

The P-T span over which biotite fluid-absent melting occurs in the present study is represented by the combination of multivariant fields of the solidus reaction (1) and the opx-in reaction (2). The position of the biotite-out

curve in figure 12 is an estimated minimum, as it was not tightly bracketed in the experiments. Fluid-absent melting involving biotite is completed over a temperature interval of 125 – 200° C during which the melt fraction increases gradually. This range is broadly consistent with the melting interval observed in other studies, except at 10 kbar where biotite persists in the run products for temperatures 50-75° C above those of previous studies (cf. Vielzeuf and Montel, 1994; Patino Douce and Beard, 1995; 1996, Stevens et al., 1997). The P-T region over which biotite, garnet and melt coexists without opx increases with pressure up to 10 kbar and then decreases, because of the slope reversal of the opx-in reaction between 10 and 15 kbar, the width of this multivariant field decreases. The interval over which biotite, opx, garnet and melt coexist is about 25 to 75° C, which is conformable with the intervals reported by Vielzeuf and Montel (1994) and Patiño Douce and Beard (1995). Patiño Douce and Beard (1996), however, found a restricted interval (25-50° C) for the coexistence of biotite, opx, garnet and melt, with the multivariant field decreasing with increasing pressure until the opx-in curve and the biotite-out curve intersects just above 10 kbar. Beyond this intersection, biotite and opx do not coexist as stable phases. This apparent discrepancy between their experiment and the present study could be due to the more ferroan nature of their biotite, which reacts out at lower temperatures forming garnet instead of opx. The results of the two studies are therefore not inconsistent. The results from my study indicate that substitution of Ti and F in biotite not only shifts the position of the fluid-absent melting reactions to higher temperatures (at

53

constant pressure) but also increases the multivariant fields between the different fluid-absent melting reactions.

Effect of Mg-number on opx formation

The two biotite in the starting materials of the present experiments differed in their Mg-number by about 10 units (PON – 0.46, KAL – 0.56). The temperature resolution in the present experiments is not enough to bring out any marked difference in the melting behavior of the two starting materials. This suggests that moderate differences in the Mg-number of biotite do not greatly affect phase relations during fluid-absent melting. Nevertheless, the partitioning of Mg into biotite relative to coexisting opx or garnet suggests that, in general, the temperature of opx formation should increase with increasing Mg-number of the starting biotite. This effect is mitigated somewhat by the influence of bulk rock Mg-number on the stability fields of garnet and opx. Decreasing bulk rock Mg-number favors the formation of garnet as the primary ferromagnesian phase associated with fluid-absent melting of biotite-bearing peraluminous rocks, and restricts opx stability to higher temperatures. The net result of these two competing factors is a relatively small influence of Mg-number on the temperature required for the first appearance of opx (cf. Patiño Douce and Beard, 1996; Stevens et al., 1997).

Granulite formation at Ponmudi and Kalanjur

The most direct application of the results of this study is in evaluating the petrogenesis of granulites at Ponmudi and Kalanjur, the two localities from which the starting materials were obtained. Many workers have interpreted the field relationships at incipient granulite localities such as these to reflect a fluid-present dehydration process, in which the breakdown of biotite or hornblende was triggered by the local influx of low water activity fluids (e.g., Janardhan et al., 1979; Ravindra Kumar et al., 1985; Ravindra Kumar and Chacko, 1986). Others, however, have argued that these or broadly similar features were the result of fluid-absent partial melting (Waters, 1988; Burton and O'Nions, 1990). The P-T position of the opx-in curve determined in the present study provides insight on the nature of the granulite-forming process at these localities.

Metamorphic P-T conditions determined for the granulites at Ponmudi and Kalanjur are 780° C, 5.2 kbar and 760° C, 5.9 kbar, respectively (Chacko et al., 1996). By comparison, extrapolation of the present experimental results to 5 to 6 kbar pressure indicates that a temperature of at least 875° C is required in order to stabilize opx by fluid-absent melting. Thus, temperature estimates for the Ponmudi and Kalanjur rocks are too low to be consistent with granulite formation by a fluid-absent melting process. One might argue that peak metamorphic temperature at these localities was in fact much higher

than ca. 780° C, but that the mineral equilibria used in calculating temperature significantly re-equilibrated during slow cooling of the rocks. However, the temperature estimates for the two localities are based on aluminium solubility in opx (the refractory garnet-Al-in-orthopyroxene thermobarometer), and are therefore likely to be a faithful representation of peak metamorphic temperature. Qualitatively, this can be corroborated by comparing the relatively low Al_2O_3 content (3.2 – 3.5 wt. %) of opx from the Ponmudi and Kalanjur granulites (Srikantappa et al., 1985; Chacko et al., 1987) to that of the opx formed at high temperature in the present experiments (5-11 wt. % Al_2O_3).

P-T estimates for the Ponmudi and Kalanjur rocks are similar to those reported for many other incipient granulite localities in South India and Sri Lanka (e.g., Srikantappa et al., 1985; Hansen et al., 1987). Thus, the conclusions drawn above likely also apply to other localities in the region where opx formed at the expense of biotite. More specifically, granulite formation at these localities did not result from fluid-absent melting, but may have been caused by the infiltration of CO_2-rich (e.g., Janardhan et al., 1979) or hypersaline fluids (Newton et al., 1998). Such fluids can induce opx growth by sub-solidus dehydration or fluid-present melting of biotite. This fluid-present mechanism of granulite formation can be evaluated further by experimentally determining the temperatures required for opx formation with the PON and KAL starting materials in the presense of carbonic or saline fluids.

Implication for the orthopyroxene isograd and deep crustal processes

If, as argued in this paper, the starting materials used in my experiments are representative of rocks found near the amphibolite- to granulite-facies transition, then the present results have important implications for the interpretation of the opx-in isograd that marks this transition. Figure 13 compares P-T constraints for opx formation derived in this study to those reported for a number of transitional amphibolite-granulite terranes worldwide. In all of these terranes, opx has been noted in rocks with bulk composition broadly similar to those investigated in the present study. My results indicate that the temperatures reported for these transitional terranes are more than 75 to 100° C lower than those required for opx formation by fluid-absent melting. These temperatures are also generally inconsistent with the opx-in curves of previous experimental studies, although the temperature discrepancy is considerably smaller in those cases.

One explanation for the large temperature discrepancy is that temperatures reported for these transitional terranes do not represent peak metamorphic temperatures. Most of the temperature estimates for the terranes shown in Figure 13 were derived from Fe-Mg exchange geothermometry, and retrograde resetting of such thermometers is known to be a common problem in high-grade, slowly cooled rocks (e.g., Frost and Chacko, 1989; Spear and Florence, 1992). Thus, it is possible that peak temperatures in these terranes were actually much higher than indicated by
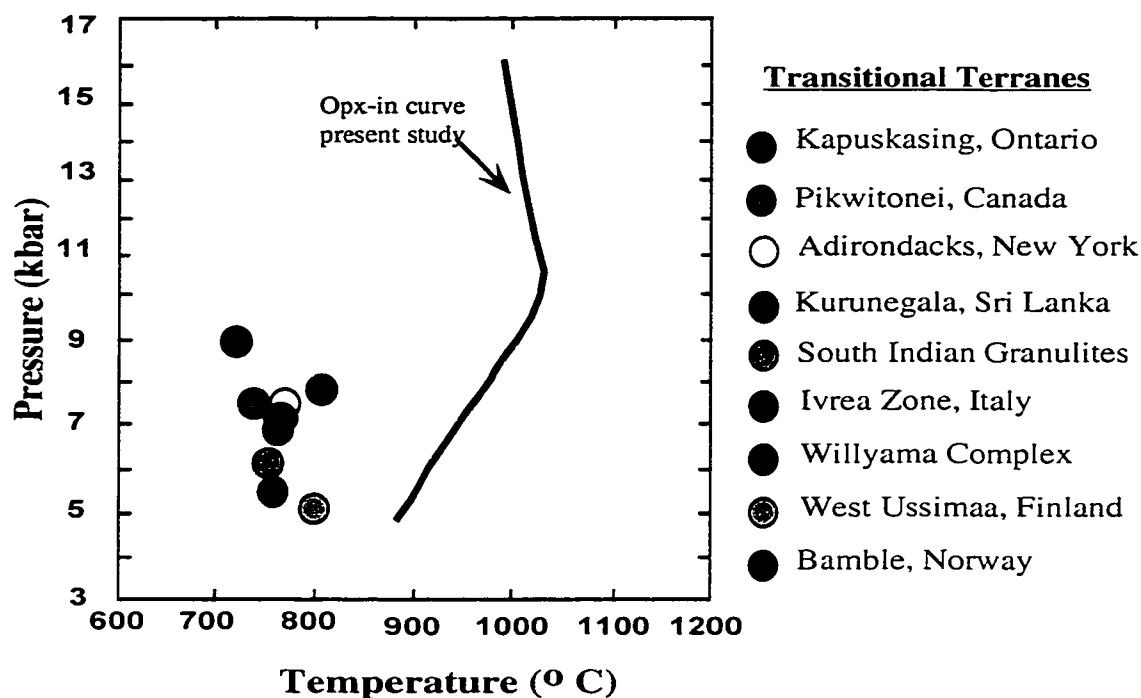
Figure 13. Comparison of peak metamorphic conditions of transitional amphibolite-granulite terranes to the P-T conditions required for orthopyroxene formation. Transitional terrane data from Janardhan et al (1982) (South India); Hansen et al. (1987) (Sri Lanka); Henk et al. (1997) (Ivrea Zone); Paktunc and Baer (1986) (Pikwitonei); Bohlen et al. (1985) (Adirondacks); Percival (1983) (Kapuskasing); Schreurs (1984) (West Ussimaa); Lamb et al. (1985) (Bamble); Phillips and Wall (1981) (Willyama Complex).

the exchange geothermometers, and comparable to those required to form opx by fluid-absent melting. This implies, however, that temperatures of crustal metamorphism commonly exceed 850 to 900° C. By comparison, existing thermal models of collisional orogenic belts suggest that temperatures in excess of 900° C are not generally achieved, even at the base of crust that has been tectonically thickened to 55 to 70 km (England and Thompson, 1984; Patiño Douce et al., 1989; Ashwal et al., 1992). Therefore, rationalization of these high temperatures either requires significant adjustment of some of the input parameters in these thermal models (e.g., values for crustal radioactive heat production), or the presence in transitional terranes of secondary heat sources such as mafic magmas.

On the other hand, if a 700 to 800° C temperature estimate for a particular transitional terrane truly represents a peak metamorphic temperature, then my results imply that opx in that terrane either formed by a process other than fluid-absent melting, or in rocks with considerably different mineral compositions than used in the present experiments. The relative merits of these alternative proposals to account for the temperature discrepancy between experimental and natural data must be evaluated on a case by case basis. Nevertheless, I suggest that the widely held notion that granulite-facies mineral assemblages develop at 700 to 800° C by fluid-absent processes be abandoned as it is inconsistent with the results of both the present and earlier experimental studies. Either temperatures in transitional

amphibolite-granulite terranes were significantly hotter than reported or the granulite-forming process was not fluid absent.

Conclusions

This study examined the fluid-absent melting behavior of two natural high-grade semi-pelitic rocks in order to constrain the P-T conditions of formation of opx. The high Ti and F contents of biotite in these rocks shifts fluid-absent melting reactions to significantly higher temperatures than reported in previous studies. Comparable results obtained on the two starting materials suggest that moderate difference in the Mg-number of biotite have no significant effect on the P-T position of the melting reactions. Fluid-absent melting of biotite in both the starting materials occurred over a multivariant region involving two main melting reactions:

$$\text{Bio + Plag + Qtz = Grt + Kfs + Melt} \quad \text{------------------- (1)}$$
$$\text{Bio + Plag + Qtz = Opx + Grt + Kfs + Melt ------------- (2)}$$
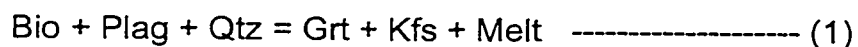
Reaction (2), the opx-in isograd, which marks the transition from amphibolite- to granulite-facies in semi-pelitic rocks, occurs at temperatures in excess of 875° C at intermediate pressures (6-8 kbar); the pressure window represented by majority of the exposed granulite-facies terranes. The typical temperatures

reported for amphibolite-granulite transition terranes are, however, considerably lower (700-850° C).

This temperature discrepancy between the experimental results and natural amphibolite-granulite transition terranes, coupled with data from thermal modeling of collisional orogens suggest that for rocks with bulk compositions similar to that of Ponmudi and Kalanjur temperatures may not have been high enough for opx formation under fluid absent conditions. Such high temperatures within the crust can be realized only through additional heat input from magma intrusion or by modifying the heat flow parameters during orogenic thickening.

Whether the amphibolite-granulite transition process operate under sub-solidus or hyper-solidus conditions, and in a fluid-present or fluid-absent environment is a matter that still needs to be understood and it is likely that each terrane is unique in the nature of the operative processes. The evidence for the involvement of hypersaline and CO_2-rich fluids in many high-grade terranes (Janardhan et al., 1982; Touret, 1985; Newton, 1986; Hansen et al., 1987; Pan and Fleet, 1996; Franz and Harlov, 1998; Nijland et al., 1998) suggests that fluid-absent conditions, after all, may not be the norm at deeper crustal levels as widely believed. Hence, more caution should be exercised in conceptualizing middle- to lower-crustal metamorphism as processes involving fluid-absent systems. Lack of adequate experimental data on the influence of sub-aqueous fluids on phase equilibria of high-grade rocks is a drawback in

modeling deep-crustal metamorphic and magmatic processes and demands more attention.

References

Abrecht, J. & Hewitt, D.A. (1988). Experimental evidence on the substitution of Ti in biotite. *American Mineralogist* **73**, 1275-1284.

Andersen, D.J., Lindsley, D.H. & Davidson, P.M. (1993). QUIIF: A Pascal program to assess equilibria among Fe-Mg-Mn-Ti oxides, pyroxenes, olivine and quartz. *Computers and Geosciences* **19**, 1333-1350.

Ashwal, L.D., Morgan, P. & Hoisch, T.D. (1992). Tectonics and heat sources for granulite metamorphism of supracrustal-bearing terranes. *Precambrian Research* **55**, 525-538.

Berman, R.G. (1988). Internally consistent thermodynamic data for stoichiometric minerals in the system $Na_2O-K_2O-Fe_2O_3-Al_2O_3-SiO_2-TiO_2-H_2O-CO_2$. *Journal of Petrology* **29**, 445-522.

Bohlen, S.R., Peacor, D.R., & Essene, E.J. (1980). Crystal chemistry of a metamorphic biotite and its significance in water barometry. *American Mineralogist* **65**, 55-62.

Bohlen, S.R., Valley, J.W., & Essene, E.J. (1985). Metamorphism in the Adirondacks:1, Petrology, pressure and temperature. *Journal of Petrology* **26**, 971-992.

Burton, K.W. & O'Nions, R.K. (1990). The timescale and mechanism of granulite formation at Kurunegala, Sri Lanka. *Contributions to Mineralogy and Petrology* **106**, 66-89.

Carrington, D.P. & Harley, S.L. (1995). Partial melting and phase relations in high-grade metapelites: an experimental petrogenetic grid in the KFMASH system. *Contributions to Mineralogy and Petrology* **120**, 270-291.

Carrington, D.P. & Watt, G.R. (1995). A geochemical and experimental study of the role of K-feldspar during water-undersaturated melting of metapelites. *Chemical Geology* **132**, 59-76.

Chacko, T. (1987). Petrologic, geochemical and isotopic studies in the charnockite-khondalite terrain of southern Kerala, India: The deposition and granulite-facies metamorphism of a Precambrian sedimentary sequence. Unpub. Ph.D thesis, University of North Carolina at Chapel Hill, 191 p.

Chacko, T., Ravindra Kumar, G.R., & Newton, R.C. (1987). Metamorphic conditions in the Kerala (south India) Khondalite Belt: a granulite-facies supracrustal terrain. *Journal of Geology* **96**, 343-358.

Chacko, T., Ravindra Kumar, G.R., Meen, J.K. & Rogers, J.J.W. (1992). Geochemistry of high-grade supracrustal rocks from the Kerala Khondalite Belt and adjacent massif charnockites, South India. *Precambrian Research* **55**, 469-489.

Chacko, T., Lamb, M. & Farquhar, J. (1996). Ultra-high temperature metamorphism in the Kerala Khondalite Belt. In: Santosh, M. &

Yoshida, M. (eds.) The Archean and Proterozoic terrains in Southern India and East Gondwana. *Gondwana Research Group Memoir* **3**, 157-165.

Clemens, J.D. (1984). Water contents of silicic to intermediate magmas. *Lithos* **17**, 273-287.

Clemens, J. D. (1992). Partial melting and granulite genesis: a partisan overview. *Precambrian Research* **55**, 297-301.

Clemens, J.D. & Vielzeuf, D. (1987). Constraints on melting and magma production in the crust. *Earth and Planetary Science Letters* **86**, 287-306.

Clemens, J.D., Droop, G.T.R. & Stevens, G. (1997). High-grade metamorphism, dehydration and crustal melting: a reinvestigation based on new experiments in the silica-saturated portion of the system $KAlO_2-MgO-SiO_2-H_2O-CO_2$ at P $\leq$1.5 GPa. *Contributions to Mineralogy and Petrology* **129**, 308-325.

Dooley, D.F. & Patiño Douce, A.E. (1996). Fluid-absent melting of F-rich phlogopite + rutile + quartz. *American Mineralogist* **81**, 202-212.

Eckert, J.O., Hatcher, R.D. & Mohr, D.W. (1989). The Wayah granulite-facies metamorphic core, southwestern North Carolina: high-grade culmination of Taconic metamorphism in the southern Blue Ridge. *Geological Society of America Bulletin* **101**, 1434-1447.

Elkins, L.T. & Grove, T.L. (1990). Ternary feldspar experiments and thermodynamic models. *American Mineralogist* **75**, 544-559.

Elvevold, S., Scrimgeour, I., Powell, R., Stuuwe, K. & Wilson, J.L. (1994). Reworking of deep-seated gabbros and associated contact metamorphosed paragneisses in the south-eastern part of the Seiland Igneous Province, northern Norway. *Journal of Metamorphic Geology* **12**, 539-556.

England, P.C. & Thompson, A.B. (1986). Some thermal and tectonic models for crustal melting in continental collision zones. In: Coward, M.P. & Ries, A.C. (eds.) Collision Tectonics. *Geological Society Special Publication* **19**, 83-94.

Forbes, W.C. & Flower, M.F.J. (1974). Phase relations of titan-phlogopite, $K_2Mg_4TiAl_2Si_6O_{20}(OH)_4$: a refractory ph ase in the upper mantle? *Earth and Planetary Science Letters* **22**, 60-66.

Franz, L. & Harlov, D.E. (1998). High-grade K-feldspar veining in granulites from the Ivrea-Verbano Zone, Northern Italy: fluid flow in the lower crust and implications for granulite facies genesis. *Journal of Geology* **106**, 455-472.

Frost, B.R. & Chacko, T. (1989). The granulite uncertainty principle: limitations on thermobarometry in granulites. *Journal of Geology* **97**, 435-450.

Fyfe, W.S. (1973). The granulite facies, partial melting and the Archean crust: *Philosophical Transaction of Royal Society (London)* **273**, 457-461.

Ghiorso, M.S. (1990). Thermodynamic properties of hematite-ilmenite-geikielite solid solutions. *Contributions to Mineralogy and Petrology* **104**, 645-667.

Grant, J.A. & Frost, B.R. (1990). Contact metamorphism and partial melting of pelitic rocks in the aureole of the Laramie Anorthosite Complex, Morton Pass, Wyoming. *American Journal of Science* **290**, 425-472.

Guidotti, C.V. & Dyar, M.D. (1984). Ferric iron in metamorphic biotite and its petrologic and crystallochemical implications. *American Mineralogist* **76**, 161-175.

Hansen, E.C., Janardhan, A.S., Newton, R.C., Prame, W.K.B.N. & Ravindrakumar, G.R. (1987). Arrested charnockite formation in southern India and Sri Lanka. *Contributions to Mineralogy and Petrology* **96**, 225-244.

Henk, A., Franz, L., Teufel, S., & Oncken, O. (1997). Magmatic underplating, extension and crustal reequilibration – insights from a cross section through the Ivrea Zone and Strona-Ceneri Zone/ northern Italy. *Journal of Geology* **105**, 367-377.

Janardhan, A.S., Newton, R.C., & Smith, J.V. (1979). Ancient crustal metamorphism at low P_{H2O}: charnockite formation at Kabbaldurga, south India. *Nature* **278**, 511-514.

Janardhan, A.S., Newton, R.C. & Hansen, E.C. (1982). The transformation of amphibolite facies gneiss to charnockite in southern Karnataka and northern Tamil Nadu, India. *Contributions to Mineralogy and Petrology* **79**, 130-149.

Johannes, W. (1984). Beginning of melting in the granite system Qz-Or-Ab-An-H_2O. *Contributions to Mineralogy and Petrology* **86**, 264-273.

Kushiro, I. (1976). A new furnace assembly with a small temperature gradient in solid-media, high pressure apparatus. *Carnegie Institution of Washington Yearbook* **68**, 231-233.

Lamb, R.C., Smalley, P.C., & Field,D. (1986). P-T condition for the Arendal granultes, southern Norway; implications for the roles of P, T, and CO_2 in deep crustal LILE-depletion. *Journal of Metamorphic Geology* **4**, 143-160.

Le Breton, N. & Thompson, A.B. (1988). Fluid-absent (dehydration) melting of biotite in metapelites in the early stages of crustal anatexis. *Contributions to Mineralogy and Petrology* **99**, 226-237.

Mattioli, G.S. & Bishop, F.C. (1984). Experimental investigation of the chromium-aluminium mixing parameter in garnet. *Geochimica et Cosmochimica Acta* **48**, 1367-1371.

Montel, J.M. & Vielzeuf, D. (1997). Partial melting of metagreywackes, Part 2. Compostions of minerals and melts. *Contributions to Mineralogy and Petrology* **128**, 176-196.

Newton, R.C. (1986). Fluids of granulite facies metamorphism. In: Walther, J.V., and Wood, B.J. (eds.) Fluid-rock interactions during metamorphism. *Springer-Verlag,* Berlin, 36-59.

Newton, R.C., Aranovich, L.Ya., Hansen, E.C. & Vandenheuvel, B.A. (1998). Hypersaline fluids in Precambrian deep-crustal metamorphism. *Precambrian Research* **91**, 41-63.

Nijland, T.G., Touret, J.L.R. & Visser, D. (1998). Anomalously low temperature orthopyroxene, spinel, and sapphirine occurrences in

metasediments from the Bamble amphibolite-to-granulite facies transition zone (South Norway): Possible evidence for localized action of saline fluids. *Journal of Geology* **106**, 575-590.

Paktunc, A.D. & Baer, A.J. (1986). Geothermobarometry of the northwestern margin of the Superior Province: Implications for its tectonic evolution. *Journal of Geology* **94**, 381-394.

Pan, Y., Fleet, M.E., & Williams, H.R. (1994). Granulite-facies metamorphism in the Quetico Subprovince, north of Manitouwadge, Ontario. *Canadian Journal of Earth Sciences* **31**, 1427-1439.

Pan, Y., and Fleet, M.E. (1996). Rare earth element mobility during prograde granulite facies metamorphism: significance of fluorine. *Contributions to Mineralogy and Petrology* **123**, 251-262.

Patiño Douce, A.E. (1993). Titanium substitution in biotite: An empirical model with applications to thermometry, O_2 and H_2O barometries, and consequences for biotite stability. *Chemical Geology* **108**, 133-162.

Patiño Douce, A.E., Humphreys, E.D. & Johnston, A.D. (1989). Anatexis and metamorphism in tectonically thickened continental crust exemplified by the Sevier hinterland, western North America. *Earth and Planetary Science Letters* **97**, 290-315.

Patiño Douce, A.E. & Johnston, A.D. (1991). Phase equilibria and melt productivity in the pelitic system: implications for the origin of peraluminous granitoids and aluminous granulites. *Contributions to Mineralogy and Petrology* **107**, 202-218.

Patiño Douce, A.E. & Beard, J.S. (1994). H$_2$O loss from hydrous melts during fluid-absent piston-cylinder experiments. *American Mineralogist* **79**, 585-588.

Patiño Douce, A.E. & Beard, J.S. (1995). Dehydration-melting of biotite gneiss and quartz amphibolite from 3 to 15 kbar. *Journal of Petrology* **36**, 707-738.

Patiño Douce, A.E. & Beard, J.S. (1996). Effects of P, f(O$_2$) and Mg/Fe ratio on dehydration melting of model metagreywackes. *Journal of Petrology* **37**, 999-1024.

Patiño Douce, A.E. & Harris N. (1998). Experimental constraints on Himalayan Anatexis. *Journal of Petrology* **39**, 689-710.

Percival, J.A. (1983). High-grade metamorphism in the Chapleau-Foleyet Area, Ontario. *American Mineralogist* **68**, 667-686.

Peterson, J.W., Chacko, T. & Kuehner, S.M. (1991). The effects of fluorine on the vapor-absent melting of phlogopite + quartz: implications for deep crustal processes. *American Mineralogist* **76**, 470-476.

Phillips, G.N. & Wall, V.J. (1981). Evaluation of prograde regional metamorphic conditions, their implications for the heat source and water activity during metamorphism in the Willyama Complex, Broken Hill, Australia. *Bulletin de Mineralogie* **104**, 810-810.

Pickering, J.M. & Johnston, A.D. (1998). Fluid-absent melting behavior of a two-mica metapelite: experimental constraints on the origin of Black Hills granite. *Journal of Petrology* **39**, 1788-1804.

Ravindra Kumar, G.R. & Chacko, T. (1986). Mechanisms of charnockite formation and break down in Southern Kerala: implications for the origin of the South Indian granulite terrain. *Journal of Geological Society of India* **28**, 277-288.

Ravindra Kumar, G.R., Srikantappa, C. & Hansen, E.C. (1985). Charnockite formation at Ponmudi in southern Kerala. *Nature* **313**, 207-209.

Rosenberg, P.E. & Foit, F.E., Jr. (1977). Fe^{2+}- F avoidance in silicates. *Geochimica et Cosmochimica Acta* **41**, 345-346.

Rutter, M.J. & Wyllie, P.J. (1988). Melting of vapour-absent tonalite at 10 kbar to simulate dehydration-melting in the deep crust. *Nature* **331**, 159-160.

Sack, R.O. & Ghiorso, M.S. (1989). Importance of considerations of mixing properties in establishing an internally consistent thermodynamic database: thermochemistry of minerals in the system Mg_2SiO_4-Fe_2SiO_4-SiO_2. *Contributions to Mineralogy and Petrology* **102**, 41-68.

Santosh, M. & Yoshida, M. (1992). A petrologic and fluid inclusion study of charnockites form the Lutzow-Holm Bay region, East Antarctica: evidence for fluid-rich metamorphism in the lower-crust. *Lithos* **29**, 107-126.

Schreurs, J. (1985). Prograde metamorphism of metapelites, garnet-biotite thermometry and prograde changes of biotite chemistry in high-grade rocks of West Uusimaa, southwest Finland. *Lithos* **18**, 69-80.

Skjerlie, K.P. & Johnston, A.D. (1993). Vapor-absent melting at 10 kbar of biotite- and amphibole-bearing tonalitic gneiss: implication for the generation of A-type granites. *Geology* **20**, 263-266.

Skjerlie, K.P., Patiño Douce, A.E. & Johnston, A.D. (1993). Fluid-absent melting of a layered crustal protolith: implications for the generation of anatectic granites. *Contributions to Mineralogy and Petrology* **114**, 365-378.

Spear, F.S. & Florence, F.P. (1992). Thermobarometry in granulites: pitfalls and new approaches. *Precambrian Research* **55**, 209-241.

Srikantappa, C., Raith, M. & Spiering, B. (1985). Progressive charnockitisation of a leptynite-khondalite suite in southern Kerala, India – evidence for formation of the charnockites through decrease in fluid pressure? *Journal of Geological Society of India* **26**, 849-872.

Stevens, G., Clemens, J.D. & Droop, G.T.R. (1997). Melt production during granulite-facies anatexis: experimental data from "primitive" metasedimentary protoliths. *Contributions to Mineralogy and Petrology* **128**, 352-370.

Thompson, A.B. (1982). Dehydration-melting of pelitic rocks and the generation of H_2O-undersaturated granitic liquids. *American Journal of Science* **282**, 1567-1595.

Touret, J.L.R. (1985). Fluid regime in southern Norway: The record of fluid inclusions. In: Tobi, A.C. & Touret, J.L.R. (eds.) The Deep Proterozoic Crust in the North Atlantic Provinces: Reidel, Dordrecht, 517-549.

Trønnes, R.G., Edgar, A.D., and Arima, M. (1985). A high pressure-high temperature study of TiO_2 solubility in Mg-rich phlogopite: implications to phlogopite chemistry. *Geochimica et Cosmochimica Acta* **49**, 2323-2329.

Truckenbrodt, J., & Johannes, W. (1999). H_2O loss during piston-cylinder experiments. *American Mineralogist* **84**, 1333-1335.

Vielzeuf, D. & Holloway, J.R. (1988). Experimental determination of the fluid-absent melting relations in the pelitic system. Consequences for crustal differentiation. *Contributions to Mineralogy and Petrology* **98**, 257-276.

Vielzeuf, D. & Montel, J.M. (1994). Partial melting of metagreywackes. 1. Fluid-absent experiments and phase relationships. *Contributions to Mineralogy and Petrology* **117**, 375-393.

Waters, D.J. (1988). Partial melting and the formation of granulite facies assemblages in Namaqualand, South Africa. *Journal of Metamorphic Geology* **6**, 387-404.

Windom, K.E., & Boettcher, A.L. (1976). The effect of reduced activity of anorthite on the reaction grossular + quartz = anorthite + wollastonite: a model for plagioclase in the earth's lower crust and upper mantle. *American Mineralogist* **61**, 889-896.

Young, D.A. (1995). Kornerupine-group minerals in Grenville granulite-facies paragneiss, Reading Prong, New Jersey. *Canadian Mineralogist* **33**, 1255-1262.

Appendix 1
Pressure Calibration

The reaction,

$$Ca_3Al_2Si_3O_{12} + SiO_2 = CaAl_2Si_2O_8 + 2\ CaSiO_3 \text{------ (1)}$$

| Grossular | Quartz | Anorthite | Wollastonite |

was used to check the pressure calibration of the piston-cylinder apparatus on which the fluid-absent experiments were performed.

Starting material

The starting materials (provided by Professor Robert Luth) for the calibration experiments was a synthetic mixture containing 68.54 mg of grossular (synthesized from stoichiometric glass with 3 wt.% H_2O at 20 kbar and 1000° C for 8 hours), 9.22 mg of quartz, 42.43 mg of anorthite (crystallized from stoichiometric glass at 1 atm. and 1400° C for 48 hours) and 35.32 mg of wollastonite (crystallized from $CaCO_3$ + SiO_2 mix which was heated in increments at 600° C (3 hours),1150° C (17 hours) and at 1625° C (1.5 hours). The quenched product was ground and heated again at 550° C (1 hour) and then at 1150° C (17 hours) (Luth, pers. comm.). This was quenched and ground and finally heated at 1150° C for 24 hours). Approximately 10 mg of the mixture was used in each experiment.

Experimental approach

The same experimental procedure was followed for the calibration experiments as in the fluid-absent experiments (3/4-inch assembly, NaCl – pyrex pressure medium, gold capsules, hot piston-out etc.). However, the samples were breath moistened before each experiment (by breathing into the capsule containing the sample before the final welding). The starting materials were characterised by X-ray diffraction. Experiments were conducted at 1000° C and at 12 and 13 kbar for one week. After quenching the capsules were

73

checked for tear. The run products recovered from the capsule were ground in an agate mortar. The powder was then characterised by X-ray diffraction. The diffractogram was compared with that of the starting mixture to ascertain the direction of the reaction progress. Reaction direction was determined by large (>40%) changes in the ratios of the strengths of anorthite and grossular peaks of the run products compared to that of the starting mixture. The strong reflections of anorthite at d=3.18 was compared to the reflections of grossular at d= 2.65. The wollastonite peaks were not used because of possible changes in peak heights due to orientation effects. Gold was the only extraneous phase observed in the quenched charges, which might have been introduced into the charge during the recovery of the sample from the gold capsules. The pressure bracket at 1000° C was compared with the position of (1) determined by Mattioli and Bishop (1984) and Windom and Boettcher (1976) (Fig. A1).
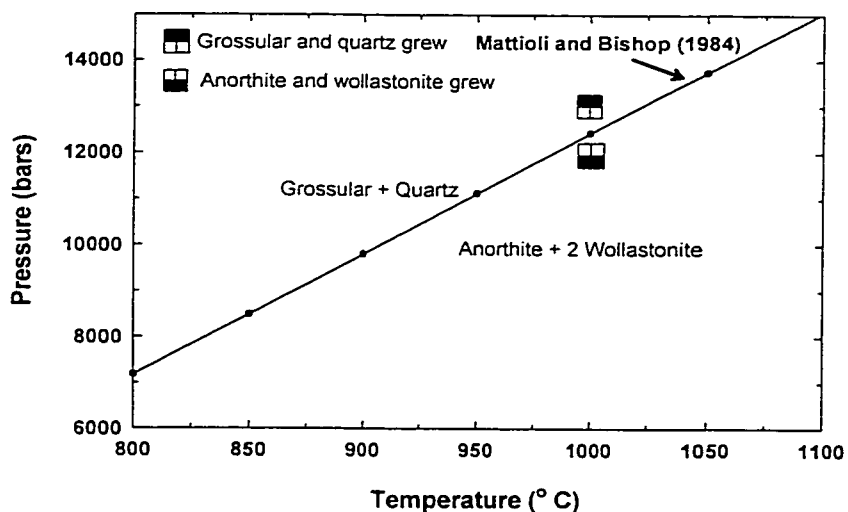
Figure A1. Pressure bracket obtained for the reaction grossular +quartz = anorthite + 2 wollastonite at 1000° C. P-T position of the univariant curve from Mattioli and Bishop (1984).

Conclusion

The pressure bracket obtained for reaction (1) is in agreement within errors to the position of the reaction reported in previous experiments. There are no discernible friction or anvil effects in this piston-cylinder assembly using salt pressure media at 1000° C. Therefore, no pressure correction was applied to the nominal pressures during the fluid-absent experiments. The reported pressures are considered to be accurate within 500 bars.

APPENDIX 2
Standards used for EPMA analyses

Element Mineral	Si	Al	Fe	Mg	Mn	Ti	Ca	Na	K	Cr	Ba	F	Cl
Biotite	Calbiotite rvgarl	Muscovite rvgarl	Calbiotite Fayalite	Calbiotite rvgarl	Willemite	Kaersutite	Kaersutite rvgarl	Kaersutite	Calbiotite	n.a.	Sanidine	CalBiotite	Tugtupite n.a.
Garnet	Sanidine	Plagioclase	Osumilite	Osumilite	Willemite	Kaersutite	rvgarl	n.a.	n.a.	n.a.	n.a.	n.a.	n.a.
Plagioclase	Sanidine	Plagioclase	Osumilite	Osumilite	Willemite	Kaersutite	Plagioclase	Albite	Sanidine	n.a.	n.a	n.a.	n.a.
Alkali-Feldspar	Augite	Augite	Osumilite	Hypersthene	Willemite	Kaersutite	Plagioclase	Albite	Sanidine	n.a.		n.a.	n.a.
Orthopyroxene	Diopside	n.a.	Grunerite	Hypersthene ncchromite	Willemite	Rutile	Augite	Kaersutite	Kaersutite	Chromite	n.a.	n.a.	n.a.
Ilmenite	Indian Basalt	Indian Basalt	Ilmenite	ncchromite	Willemite	Hawaiian Basalt	Diopside	n.a.	n.a.	ncchromite	n.a	n.a.	n.a.
Glass		Indian Basalt	Indian Basalt	Indian Basalt	Willemite	Indian Basalt	Indian Basalt	Rhyolite	Rhyolite	n.a.	n.a.	n.a.	n.a.

In addition v_metal and galnnite was used as a standard for V and Zn,respectively, for ilmenite analyses.

76

Run No.	RJ-5	RJ-3	RJ-33	RJ-11	RJ-9	RJ-25	RJ-17	RJ-15	RJ-13	RJ-23	RJ-19	RJ-21
n	11	14	20	17	13	14	20	38	20	19	14	14
P (kbar)	7	7	7	7	7	7	10	10	10	10	15	15
T (°C)	800	850	875	900	950	1000	875	900	950	1000	950	1000
SiO_2	37.42	38.13	37.64	37.62	38.37	37.10	38.04	37.70	38.11	37.30	37.69	38.35
TiO_2	5.50	5.00	5.02	5.41	5.79	6.52	5.37	5.39	5.70	6.01	5.18	5.44
Al_2O_3	13.58	14.52	15.64	14.15	14.43	13.13	16.10	15.81	15.14	13.71	14.30	13.94
FeO^*	19.72	18.14	19.37	16.03	15.15	15.17	17.78	18.24	16.51	14.76	17.29	13.56
MnO	0.06	0.05	0.03	0.02	0.04	0.04	0.03	0.04	0.03	0.04	0.03	0.03
MgO	10.33	10.74	9.94	13.41	13.33	12.69	10.18	10.25	11.53	12.97	10.52	13.40
CaO	0.02	0.02	0.04	0.06	0.07	0.11	0.03	0.03	0.05	0.06	0.07	0.06
Na_2O	0.29	0.30	0.45	0.46	0.53	0.52	0.31	0.38	0.44	0.52	0.45	0.48
BaO	0.25	0.20	n.d.	0.21	0.27	0.24	0.22	0.23	0.25	0.27	0.21	0.22
K2O	9.36	9.60	9.41	9.51	9.54	8.75	9.75	9.62	9.56	9.44	9.64	9.67
F	1.81	1.91	2.20	3.64	2.50	3.14	1.84	1.67	1.84	3.07	2.84	3.64
Cl	0.36	0.33	0.33	0.36	0.22	0.22	0.33	0.31	0.26	0.15	0.30	0.22
O=F	0.76	0.80	0.93	1.53	1.05	1.32	0.78	0.70	0.77	1.29	1.20	1.53
O=Cl	0.08	0.07	0.08	0.08	0.05	0.05	0.07	0.07	0.06	0.03	0.07	0.05
Total	97.85	98.05	99.07	99.26	99.12	96.25	99.14	98.88	98.58	96.98	97.26	97.42
Cations 22 (O)												
Si	5.540	5.575	5.457	5.356	5.466	5.431	5.487	5.473	5.502	5.425	5.524	5.494
Ti	0.613	0.550	0.547	0.579	0.620	0.718	0.583	0.589	0.619	0.658	0.571	0.586
Al	2.369	2.502	2.671	2.374	2.423	2.264	2.737	2.705	2.576	2.35	2.469	2.353
Fe	2.441	2.218	2.347	1.908	1.804	1.857	2.144	2.214	1.993	1.795	2.118	1.624
Mn	0.007	0.006	0.004	0.003	0.004	0.005	0.004	0.004	0.003	0.005	0.004	0.003
Mg	2.280	2.340	2.149	2.846	2.832	2.769	2.190	2.218	2.482	2.812	2.298	2.862
Ca	0.002	0.003	0.006	0.010	0.010	0.017	0.005	0.005	0.008	0.01	0.011	0.009
Na	0.084	0.085	0.127	0.126	0.147	0.147	0.088	0.106	0.122	0.145	0.129	0.134
Ba	0.015	0.011	n.d.	0.012	0.015	0.014	0.012	0.013	0.014	0.015	0.012	0.012
K	1.768	1.790	1.739	1.726	1.733	1.633	1.794	1.781	1.761	1.751	1.802	1.766
F	0.849	0.883	1.010	1.640	1.128	1.454	0.841	0.768	0.839	1.411	1.318	1.649
Cl	0.090	0.082	0.082	0.087	0.052	0.054	0.080	0.076	0.064	0.038	0.074	0.054
OH**	3.061	3.035	2.908	2.273	2.820	2.492	3.079	3.156	3.097	2.551	2.608	2.297
X_f	0.212	0.221	0.253	0.410	0.282	0.364	0.210	0.192	0.210	0.353	0.330	0.412
X_{Mg}	0.483	0.513	0.478	0.599	0.611	0.599	0.505	0.500	0.555	0.610	0.520	0.638

n - number of analyses; * - total Fe measured as FeO; n.a. - not analysed; n.d. - not determined; X_f =(F/(F+Cl+OH)) molar; X_{Mg} - molar (Mg/(Mg + Fe)).
** - calculated by difference.

77

APPENDIX 3B
Biotite Compositions (Kalanjur)

Sample No.	RJ-6	RJ-4	RJ-34	RJ-12	RJ-10	RJ-18	RJ-16	RJ-14	RJ-24	RJ-20	RJ-22
n	19	10	7	16	6	10	24	6	5	30	4
P (kbar)	7	7	7	7	7	10	10	10	10	15	15
T (°C)	800	850	875	900	950	875	900	950	1000	950	1000
SiO_2	37.24	37.59	37.70	37.77	38.36	37.41	36.98	38.25	36.75	37.66	37.77
TiO_2	5.61	5.63	5.31	5.76	6.15	5.54	5.66	5.84	6.64	5.26	5.63
Al_2O_3	14.02	14.56	16.03	15.43	15.01	15.88	14.58	15.49	13.82	14.54	14.15
FeO*	15.93	15.67	17.38	14.23	12.91	17.46	18.38	14.99	13.74	15.73	12.45
MnO	0.04	0.05	0.05	0.05	0.08	0.04	0.05	0.03	0.04	0.03	0.03
MgO	12.40	12.47	10.93	13.76	14.99	11.22	11.74	12.29	13.67	12.02	13.80
CaO	0.03	0.00	0.05	0.05	0.06	0.05	0.04	0.04	0.08	0.05	0.06
Na_2O	0.29	0.27	0.42	0.45	0.41	0.36	0.42	0.40	0.52	0.42	0.44
BaO	0.25	0.26	n.a.	0.27	0.30	0.23	0.27	0.27	0.35	0.30	0.30
K2O	9.85	9.82	9.48	9.80	9.84	9.66	9.54	9.52	9.33	9.76	9.65
F	1.19	1.49	1.61	2.93	2.18	1.00	0.87	1.35	2.49	2.54	2.92
Cl	0.30	0.40	0.31	0.37	0.29	0.35	0.30	0.24	0.16	0.37	0.22
O=F	0.50	0.63	0.68	1.23	0.92	0.42	0.37	0.57	1.05	1.07	1.23
O=Cl	0.07	0.09	0.07	0.08	0.07	0.08	0.07	0.05	0.04	0.08	0.05
Total	96.58	97.50	98.51	99.56	99.59	98.69	98.40	98.08	96.49	97.53	96.14
Cations 22 (O)											
Si	5.522	5.497	5.460	5.336	5.401	5.447	5.444	5.518	5.370	5.481	5.481
Ti	0.625	0.619	0.578	0.611	0.651	0.607	0.627	0.633	0.730	0.576	0.615
Al	2.450	2.509	2.737	2.570	2.491	2.725	2.529	2.634	2.379	2.493	2.420
Fe	1.975	1.917	2.105	1.681	1.520	2.125	2.263	1.809	1.679	1.914	1.511
Mn	0.005	0.006	0.006	0.006	0.009	0.004	0.006	0.003	0.005	0.004	0.004
Mg	2.742	2.719	2.359	2.899	3.145	2.434	2.576	2.643	2.977	2.608	2.985
Ca	0.005	0.000	0.008	0.008	0.008	0.008	0.007	0.007	0.013	0.008	0.010
Na	0.082	0.077	0.119	0.123	0.112	0.100	0.119	0.111	0.146	0.120	0.123
Ba	0.014	0.015	n.d.	0.015	0.017	0.013	0.015	0.015	0.020	0.017	0.017
K	1.863	1.832	1.751	1.767	1.767	1.793	1.791	1.751	1.739	1.811	1.786
F	0.559	0.689	0.738	1.308	0.971	0.460	0.407	0.617	1.152	1.170	1.339
Cl	0.076	0.098	0.075	0.088	0.070	0.086	0.076	0.058	0.040	0.092	0.053
OH**	3.365	3.212	3.187	2.604	2.958	3.454	3.517	3.325	2.808	2.738	2.608
X_F	0.140	0.172	0.185	0.327	0.243	0.115	0.102	0.154	0.288	0.293	0.335
X_{Mg}	0.581	0.587	0.528	0.633	0.674	0.534	0.532	0.594	0.639	0.577	0.664

APPENDIX 4A
Garnet Compositions (Ponmudi)

Run No.	RJ-5	RJ-3	RJ-33	RJ-11	RJ-9	RJ-25	RJ-17	RJ-15	RJ-13	RJ-23	RJ-31	RJ-19	RJ-21	RJ-29
n	10	10	10	10	10	10	9	10	10	10	10	14	10	5
P(kbar)	7	7	7	7	7	7	10	10	10	10	10	15	15	15
T(°C)	800	850	875	900	950	1000	875	900	950	1000	1050	950	1000	1050
SiO_2	37.37	37.37	37.12	37.49	37.78	37.34	37.59	37.81	37.68	37.72	37.92	36.86	37.50	37.85
TiO_2	0.03	0.11	0.09	0.05	0.12	0.16	0.08	0.13	0.12	0.21	0.61	0.05	0.31	1.00
Al_2O_3	21.10	21.50	21.28	21.51	21.45	21.28	21.42	21.43	21.41	21.57	21.45	21.22	21.53	21.19
FeO^*	33.89	33.63	33.70	33.59	32.90	32.48	33.51	33.28	32.88	32.03	28.90	33.60	31.74	24.79
MnO	0.70	0.66	0.64	0.65	0.60	0.66	0.60	0.62	0.63	0.61	0.46	0.65	0.55	0.22
MgO	3.38	3.52	3.66	3.58	3.91	4.46	3.80	3.75	3.86	4.81	6.89	3.65	4.68	8.35
CaO	2.40	2.29	2.45	2.30	2.22	2.41	2.46	2.32	2.30	2.37	2.37	2.44	2.96	4.38
Total	98.87	99.07	98.93	99.18	98.98	98.79	99.47	99.33	98.89	99.31	98.61	98.47	99.27	97.78
Cations 12 (O)														
Si	3.017	3.004	2.994	3.009	3.025	2.997	3.007	3.022	3.022	3.000	2.993	2.989	2.987	2.974
Ti	0.002	0.006	0.005	0.003	0.007	0.010	0.005	0.008	0.007	0.012	0.036	0.003	0.019	0.059
Al	2.008	2.037	2.023	2.034	2.024	2.013	2.019	2.019	2.023	2.022	1.995	2.028	2.021	1.962
Fe	2.288	2.260	2.273	2.254	2.203	2.181	2.242	2.224	2.205	2.130	1.907	2.278	2.113	1.629
Mn	0.048	0.045	0.044	0.044	0.041	0.045	0.041	0.042	0.043	0.041	0.031	0.045	0.037	0.015
Mg	0.406	0.422	0.440	0.429	0.467	0.533	0.453	0.447	0.461	0.570	0.811	0.441	0.556	0.978
Ca	0.208	0.197	0.211	0.198	0.191	0.207	0.211	0.198	0.197	0.202	0.201	0.211	0.252	0.369
X_{alm}	0.776	0.773	0.766	0.771	0.759	0.735	0.761	0.764	0.759	0.724	0.646	0.766	0.714	0.545
X_{sps}	0.016	0.015	0.015	0.015	0.014	0.015	0.014	0.014	0.015	0.014	0.011	0.015	0.013	0.005
X_{prp}	0.138	0.144	0.148	0.147	0.161	0.180	0.154	0.154	0.159	0.194	0.275	0.148	0.188	0.327
X_{grs}	0.071	0.067	0.071	0.068	0.066	0.070	0.072	0.068	0.068	0.069	0.068	0.071	0.085	0.123
X_{Mg}	0.151	0.157	0.162	0.160	0.175	0.196	0.168	0.167	0.173	0.211	0.298	0.162	0.208	0.375

X_{alm} - molar (Fe/(Fe + Mg + Ca + Mn)); X_{sps} - molar (Mn/(Fe + Mg + Ca + Mn)); X_{grs} - molar (Ca/(Fe + Mg + Ca + Mn)); Xpy - molar (Mg/(Fe + Mg + Ca + Mn))

APPENDIX 4B
Garnet Compositions (Kalanjur)

Run No.	RJ-6	RJ-4	RJ-34	RJ-12	RJ-10	RJ-26	RJ-18	RJ-16	RJ-14	RJ-24	RJ-32	RJ-20	RJ-22	RJ-30
n	8	10	10	10	15	10	10	10	10	10	9	10	14	12
P(kbar)	7	7	7	7	7	7	10	10	10	10	10	15	15	15
T(°C)	800	850	875	900	950	1000	875	900	950	1000	1050	950	1000	1050
SiO_2	38.07	37.77	37.89	38.52	38.17	38.18	37.61	38.31	38.54	38.75	38.13	38.23	38.06	37.43
TiO_2	0.11	0.04	0.11	0.06	0.07	0.11	0.08	0.07	0.09	0.08	0.52	0.10	0.21	0.20
Al_2O_3	21.86	21.75	21.89	22.06	21.63	21.90	21.81	21.96	21.91	21.85	21.88	22.05	21.86	21.86
FeO^{**}	30.19	30.26	30.66	28.88	30.38	29.96	30.59	30.30	30.04	29.43	26.86	29.96	29.28	30.08
MnO	0.66	0.70	0.68	0.68	0.70	0.70	0.68	0.63	0.65	0.64	0.55	0.69	0.59	0.63
MgO	6.29	6.24	6.42	7.29	6.32	6.70	6.30	6.37	6.42	7.14	8.71	6.59	6.81	6.53
CaO	1.66	1.72	1.78	1.71	1.72	1.82	1.78	1.68	1.69	1.83	1.95	1.76	2.17	1.99
Total	98.84	98.47	99.43	99.19	98.98	99.37	98.86	99.32	99.34	99.71	98.58	99.38	98.97	98.71
Cations 12(O)														
Si	3.007	3.000	2.985	3.01	3.015	2.998	2.982	3.011	3.023	3.020	2.977	3.000	2.994	2.968
Ti	0.007	0.002	0.006	0.004	0.004	0.006	0.005	0.004	0.005	0.004	0.030	0.006	0.012	0.012
Al	2.035	2.036	2.033	2.032	2.013	2.027	2.038	2.034	2.025	2.006	2.013	2.039	2.027	2.042
Fe	1.994	2.009	2.019	1.887	2.006	1.967	2.028	1.991	1.97	1.918	1.753	1.966	1.926	1.995
Mn	0.044	0.047	0.045	0.045	0.047	0.046	0.046	0.042	0.043	0.042	0.036	0.046	0.039	0.042
Mg	0.741	0.739	0.754	0.849	0.744	0.785	0.745	0.746	0.750	0.830	1.013	0.771	0.799	0.772
Ca	0.140	0.146	0.150	0.143	0.145	0.153	0.151	0.141	0.142	0.153	0.163	0.148	0.183	0.169
X_{alm}	0.683	0.683	0.680	0.645	0.682	0.667	0.777	0.682	0.678	0.652	0.591	0.671	0.654	0.670
X_{sps}	0.015	0.016	0.015	0.015	0.016	0.016	0.017	0.014	0.015	0.014	0.012	0.016	0.013	0.014
X_{prp}	0.254	0.251	0.254	0.290	0.253	0.266	0.160	0.255	0.258	0.282	0.342	0.263	0.271	0.259
X_{grs}	0.048	0.050	0.051	0.049	0.049	0.052	0.045	0.048	0.049	0.052	0.055	0.050	0.062	0.057
X_{Mg}	0.729	0.731	0.728	0.690	0.729	0.715	0.829	0.727	0.724	0.698	0.634	0.718	0.707	0.721

80

APPENDIX 5A
Plagioclase Compositions (Ponmudi)

Run No.	RJ-5	RJ-3	RJ-33	RJ-11	RJ-9	RJ-25	RJ-17	RJ-15	RJ-13	RJ-23	RJ-31	RJ-19	RJ-21	RJ-29
n	11	9	11	13	16	22	20	19	24	19	17	19	20	23
P (kbar)	7	7	7	7	7	7	10	10	10	10	10	15	15	15
T (°C)	800	850	875	900	950	1000	875	900	950	1000	1050	950	1000	1050
SiO_2	60.32	60.14	60.10	60.00	60.20	58.59	60.46	60.40	60.02	58.54	60.22	60.46	60.57	59.78
TiO_2	0.04	0.02	0.03	0.03	0.05	0.02	0.03	0.02	0.01	0.02	0.03	0.03	0.02	0.02
Al_2O_3	25.08	25.03	25.08	24.77	24.94	25.27	24.95	25.18	24.79	25.22	24.84	24.53	25.03	25.09
FeO	0.18	0.23	0.33	0.29	0.31	0.29	0.30	0.31	0.26	0.27	0.34	0.32	0.28	0.29
MnO	0.01	0.01	0.01	0.00	0.01	0.00	0.01	0.01	0.01	0.01	0.01	0.01	0.00	0.01
MgO	0.00	0.00	0.00	0.00	0.07	0.01	0.01	0.01	0.01	0.01	0.03	0.01	0.02	0.01
CaO	6.59	6.50	6.53	6.71	6.64	6.96	6.59	6.71	6.51	6.83	6.69	6.63	6.49	6.69
Na_2O	7.67	7.31	6.83	6.63	6.25	6.10	6.85	6.51	6.79	6.21	5.79	6.51	6.43	5.98
K_2O	0.25	0.50	1.37	1.40	1.84	1.91	1.14	1.41	1.37	1.94	2.35	1.53	1.76	2.04
Total	100.13	99.75	100.27	99.83	100.32	99.14	100.33	100.54	99.78	99.06	100.31	100.02	100.60	99.92
Cations 8 (O)														
Si	2.683	2.686	2.681	2.688	2.686	2.652	2.691	2.684	2.689	2.653	2.691	2.702	2.692	2.680
Ti	0.001	0.001	0.001	0.001	0.002	0.001	0.001	0.001	0.000	0.001	0.001	0.001	0.001	0.001
Al	1.315	1.318	1.318	1.308	1.311	1.348	1.309	1.319	1.309	1.347	1.308	1.292	1.311	1.325
Fe	0.007	0.009	0.012	0.011	0.012	0.011	0.011	0.012	0.010	0.010	0.013	0.012	0.010	0.011
Mn	0.000	0.000	0.000	0.000	0.000	0.000	0.000	0.000	0.000	0.000	0.000	0.000	0.000	0.000
Mg	0.000	0.000	0.000	0.000	0.005	0.000	0.000	0.001	0.001	0.001	0.002	0.001	0.001	0.001
Ca	0.314	0.311	0.312	0.322	0.318	0.337	0.314	0.319	0.312	0.332	0.320	0.317	0.309	0.321
Na	0.661	0.633	0.591	0.576	0.541	0.535	0.591	0.561	0.590	0.546	0.502	0.564	0.554	0.520
K	0.014	0.029	0.078	0.08	0.105	0.110	0.065	0.080	0.079	0.112	0.134	0.087	0.100	0.117
$X_{Anorthite}$	0.317	0.320	0.318	0.329	0.330	0.343	0.324	0.332	0.318	0.335	0.335	0.327	0.321	0.335
X_{Albite}	0.668	0.651	0.602	0.589	0.561	0.545	0.609	0.584	0.601	0.552	0.525	0.583	0.575	0.543
$X_{Orthoclase}$	0.014	0.030	0.080	0.082	0.109	0.112	0.067	0.083	0.081	0.113	0.140	0.090	0.104	0.122

$X_{Anorthite}$ = molar (Ca/(Ca+Na+K)); X_{Albite} = molar (Na/(Ca+Na+K)); $X_{Orthoclase}$ = molar (K/(Ca+Na+K)).

APPENDIX 5B

Plagioclase Compositions (Kalanjur)

Run No.	RJ-6	RJ-4	RJ-34	RJ-12	RJ-10	RJ-26	RJ-18	RJ-16	RJ-14	RJ-24	RJ-32	RJ-20	RJ-22	RJ-30
n	10	14	12	15	19	24	23	18	25	25	25	25	22	21
P (kbar)	7	7	7	7	7	7	10	10	10	10	10	15	15	15
T (°C)	800	850	875	900	950	1000	875	900	950	1000	1050	950	1000	1050
SiO_2	58.87	58.86	59.10	58.64	59.43	58.22	58.18	57.29	58.73	58.28	58.51	58.48	57.15	58.85
TiO_2	0.02	0.02	0.03	0.04	0.03	0.06	0.02	0.01	0.03	0.02	0.03	0.01	0.04	0.02
Al_2O_3	25.67	25.54	25.69	25.67	25.98	25.90	26.01	25.94	26.06	25.89	25.75	25.89	25.67	25.34
FeO	0.21	0.13	0.35	0.32	0.32	0.34	0.34	0.31	0.34	0.33	0.39	0.33	0.29	0.34
MnO	0.01	0.02	0.01	0.01	0.00	0.01	0.00	0.01	0.01	0.01	0.01	0.01	0.01	0.01
MgO	0.00	0.00	0.02	0.02	0.01	0.02	0.00	0.01	0.01	0.01	0.02	0.01	0.02	0.01
CaO	7.47	7.37	7.33	7.45	7.50	7.83	7.62	7.61	7.69	7.80	7.67	7.55	7.56	7.63
Na_2O	6.98	6.84	6.39	6.23	5.84	5.79	6.45	6.51	6.27	5.84	5.43	6.43	6.27	5.85
K_2O	0.50	0.49	1.20	1.32	1.49	1.68	0.97	1.02	1.34	1.79	2.02	1.28	1.38	1.66
Total	99.72	99.27	100.12	99.69	100.60	99.84	99.60	98.71	100.47	99.97	99.82	99.99	98.37	99.70
Cation 8 (O)														
Si	2.640	2.648	2.644	2.637	2.645	2.621	2.619	2.606	2.624	2.622	2.634	2.626	2.612	2.649
Ti	0.001	0.001	0.001	0.001	0.001	0.002	0.001	0.000	0.001	0.001	0.001	0.000	0.001	0.001
Al	1.356	1.354	1.355	1.360	1.362	1.374	1.38	1.391	1.372	1.373	1.366	1.370	1.382	1.344
Fe	0.008	0.005	0.013	0.012	0.012	0.013	0.013	0.012	0.013	0.012	0.015	0.012	0.011	0.013
Mn	0.000	0.001	0.000	0.000	0.000	0.001	0.000	0.000	0.000	0.000	0.000	0.000	0.000	0.000
Mg	0.000	0.000	0.001	0.001	0.001	0.002	0.000	0.001	0.000	0.001	0.001	0.001	0.001	0.001
Ca	0.359	0.355	0.351	0.359	0.358	0.378	0.367	0.371	0.368	0.376	0.370	0.363	0.370	0.368
Na	0.606	0.596	0.554	0.543	0.504	0.505	0.563	0.574	0.543	0.510	0.474	0.560	0.555	0.510
K	0.028	0.028	0.069	0.076	0.085	0.097	0.056	0.059	0.076	0.103	0.116	0.073	0.080	0.095
$X_{Anorthite}$	0.362	0.363	0.360	0.367	0.378	0.386	0.372	0.370	0.373	0.380	0.385	0.364	0.368	0.378
X_{Albite}	0.610	0.609	0.569	0.555	0.532	0.515	0.571	0.572	0.550	0.516	0.494	0.562	0.552	0.524
$X_{Orthoclase}$	0.028	0.029	0.071	0.078	0.090	0.099	0.057	0.059	0.077	0.104	0.121	0.073	0.080	0.098

82

APPENDIX 6A
Alkali feldspar Compositions (Ponmudi)

K-spar	RJ-5	RJ-3	RJ-33	RJ-11	RJ-9	RJ-25	RJ-17	RJ-15	RJ-13	RJ-23	RJ-31	RJ-19	RJ-21	RJ-29
n	11	14	17	24	13	29	31	29	27	28	21	29	25	24
P (kbar)	7	7	7	7	7	7	10	10	10	10	10	15	15	15
T (°C)	800	850	875	900	950	1000	875	900	950	1000	1050	950	1000	1050
SiO_2	64.74	64.96	64.99	65.59	65.28	66.24	65.51	65.12	65.50	65.74	65.39	65.07	65.73	65.74
TiO_2	0.03	0.05	0.03	0.05	0.04	0.04	0.04	0.04	0.04	0.03	0.06	0.04	0.04	0.03
Al_2O_3	18.94	19.02	18.97	18.89	19.01	19.08	19.04	18.88	18.94	19.02	18.92	18.83	19.22	19.23
FeO	0.23	0.22	0.26	0.28	0.22	0.27	0.29	0.29	0.26	0.25	0.30	0.27	0.24	0.27
MnO	0.00	0.01	0.01	0.01	0.01	0.01	0.01	0.01	0.01	0.01	0.01	0.01	0.00	0.01
MgO	0.00	0.00	0.00	0.00	0.00	0.00	0.01	0.01	0.00	0.00	0.01	0.00	0.00	0.01
CaO	0.19	0.24	0.47	0.41	0.52	0.46	0.39	0.40	0.49	0.59	0.80	0.49	0.63	0.77
Na_2O	2.66	2.34	2.91	2.97	2.98	3.04	2.89	2.98	2.97	3.11	3.09	3.28	3.43	3.34
K_2O	12.83	12.89	11.49	11.73	11.41	11.55	11.90	11.74	11.72	11.42	10.71	11.21	11.00	10.70
Total	99.62	99.72	99.12	99.92	99.46	100.70	100.07	99.45	99.94	100.16	99.28	99.21	100.29	100.10
Cations 8 (O)														
Si	2.974	2.977	2.981	2.987	2.982	2.988	2.981	2.982	2.983	2.983	2.985	2.982	2.976	2.977
Ti	0.001	0.002	0.001	0.002	0.001	0.001	0.001	0.001	0.001	0.001	0.002	0.001	0.001	0.001
Al	1.025	1.028	1.025	1.014	1.023	1.015	1.021	1.019	1.017	1.017	1.018	1.017	1.025	1.026
Fe	0.009	0.008	0.010	0.011	0.008	0.010	0.011	0.011	0.010	0.009	0.011	0.010	0.009	0.010
Mn	0.000	0.000	0.000	0.000	0.000	0.000	0.000	0.000	0.000	0.000	0.000	0.000	0.000	0.000
Mg	0.000	0.000	0.000	0.000	0.000	0.000	0.000	0.000	0.000	0.000	0.000	0.000	0.000	0.001
Ca	0.009	0.012	0.023	0.020	0.025	0.022	0.019	0.020	0.024	0.028	0.039	0.024	0.031	0.038
Na	0.237	0.208	0.259	0.262	0.264	0.266	0.255	0.264	0.262	0.274	0.273	0.291	0.301	0.293
K	0.752	0.753	0.672	0.681	0.665	0.665	0.691	0.685	0.681	0.661	0.624	0.655	0.635	0.618
$X_{Anorthite}$	0.009	0.012	0.024	0.021	0.026	0.023	0.020	0.021	0.025	0.029	0.042	0.025	0.032	0.040
X_{Albite}	0.237	0.214	0.271	0.272	0.277	0.279	0.264	0.272	0.271	0.285	0.292	0.300	0.311	0.309
$X_{Orthoclase}$	0.754	0.774	0.704	0.707	0.697	0.698	0.716	0.707	0.704	0.686	0.667	0.675	0.657	0.651

APPENDIX 6B

Alkali feldspar Compositions (Kalanjur)

Run No.	RJ-6	RJ-4	RJ-34	RJ-12	RJ-10	RJ-26	RJ-18	RJ-16	RJ-14	RJ-24	RJ-32	RJ-20	RJ-22	RJ-30
n	13	15	18	25	13	27	28	26	28	27	24	26	25	23
P (kbar)	7	7	7	7	7	7	10	10	10	10	10	15	15	15
T(°C)	800	850	875	900	950	1000	875	900	950	1000	1050	950	1000	1050
SiO_2	63.47	64.14	64.46	65.04	65.34	65.25	64.72	64.79	65.43	65.52	65.37	65.01	65.23	65.18
TiO_2	0.04	0.03	0.06	0.06	0.06	0.04	0.05	0.04	0.05	0.06	0.06	0.04	0.04	0.05
Al_2O_3	18.97	18.85	19.02	18.93	19.29	18.99	18.83	18.86	19.17	19.00	18.99	18.97	19.11	19.03
FeO	0.17	0.14	0.31	0.29	0.28	0.26	0.31	0.31	0.28	0.27	0.33	0.30	0.32	0.29
MnO	0.00	0.00	0.01	0.01	0.01	0.01	0.01	0.01	0.01	0.00	0.01	0.01	0.01	0.00
MgO	0.00	0.00	0.02	0.00	0.00	0.00	0.00	0.00	0.00	0.00	0.00	0.00	0.00	0.00
CaO	0.33	0.21	0.37	0.50	0.50	0.62	0.38	0.42	0.52	0.54	0.71	0.51	0.66	0.66
Na_2O	2.18	2.09	2.52	2.83	2.65	2.88	2.63	3.04	2.73	2.73	2.88	3.09	3.18	3.07
K_2O	13.30	13.74	12.29	11.83	12.03	11.60	12.19	11.61	12.06	11.69	11.12	11.55	11.16	11.03
Total	98.46	99.20	99.05	99.49	100.15	99.65	99.12	99.06	100.25	99.81	99.47	99.47	99.72	99.32
Cations 8 (O)														
Si	2.959	2.970	2.971	2.978	2.972	2.979	2.979	2.978	2.975	2.985	2.983	2.976	2.974	2.979
Ti	0.002	0.001	0.002	0.002	0.002	0.001	0.002	0.001	0.002	0.002	0.002	0.002	0.002	0.002
Al	1.042	1.029	1.033	1.022	1.034	1.022	1.022	1.022	1.027	1.020	1.021	1.023	1.027	1.025
Fe	0.007	0.006	0.012	0.011	0.011	0.010	0.012	0.012	0.010	0.010	0.013	0.011	0.012	0.011
Mn	0.000	0.000	0.000	0.000	0.000	0.000	0.000	0.000	0.000	0.000	0.000	0.000	0.000	0.000
Mg	0.000	0.000	0.001	0.000	0.000	0.000	0.000	0.000	0.000	0.000	0.000	0.000	0.000	0.000
Ca	0.016	0.010	0.018	0.024	0.024	0.031	0.019	0.021	0.026	0.026	0.035	0.025	0.032	0.032
Na	0.197	0.187	0.225	0.252	0.233	0.255	0.234	0.270	0.241	0.241	0.255	0.274	0.281	0.272
K	0.791	0.811	0.723	0.691	0.698	0.675	0.716	0.681	0.699	0.679	0.647	0.675	0.649	0.643
$X_{Anorthite}$	0.016	0.010	0.019	0.025	0.025	0.032	0.020	0.022	0.027	0.027	0.037	0.026	0.033	0.034
X_{Albite}	0.196	0.186	0.233	0.261	0.244	0.265	0.241	0.278	0.249	0.255	0.272	0.281	0.292	0.287
$X_{Orthoclase}$	0.788	0.805	0.748	0.715	0.731	0.702	0.739	0.701	0.724	0.718	0.691	0.693	0.675	0.679

APPENDIX 7
Orthopyroxene Compositions

Run No.	RJ-9	RJ-9*	RJ-25	RJ-25*	RJ-31	RJ-31*	RJ-10	RJ-10*	RJ-26	RJ-26*	RJ-32	RJ-32*
P (kbar)	7	7	7	7	10	10	7	7	7	7	10	10
T (°C)	950	950	1000	1000	1050	1050	950	950	1000	1000	1050	1050
SiO_2	52.06	48.15	47.40	44.05	50.74	48.29	52.10	50.27	48.08	48.37	50.31	44.97
TiO_2	0.80	0.83	1.49	1.62	1.01	1.09	0.40	0.35	1.47	1.38	1.18	1.29
Al_2O_3	7.95	6.82	8.49	7.62	8.67	7.94	5.77	5.09	11.31	9.76	9.95	9.00
FeO^T	26.48	29.07	26.99	29.99	23.26	25.17	23.30	24.78	23.51	23.86	21.52	24.67
MnO	0.19	0.21	0.27	0.30	0.17	0.18	0.35	0.37	0.24	0.24	0.19	0.22
MgO	12.88	14.23	14.51	16.22	15.34	16.62	17.48	18.67	15.68	16.03	16.67	19.34
CaO	0.69	0.55	0.42	0.26	0.55	0.53	0.36	0.33	0.30	0.21	0.44	0.32
Na_2O	0.45	0.13	0.25	0.00	0.35	0.16	0.17	0.09	0.25	0.10	0.30	0.13
K_2O	0.51	0.00	0.48	0.00	0.74	0.00	0.35	0.00	0.62	0.00	0.58	0.00
Cr_2O_3	0.05	0.05	0.02	0.02	0.02	0.02	0.05	0.05	0.05	0.05	0.07	0.07
Total	102.06	100.04	100.32	100.08	100.85	100.00	100.33	100.00	101.51	100.00	101.21	100.00
Cations (6O)												
Si	1.923	1.851	1.809	1.718	1.882	1.823	1.936	1.892	1.778	1.808	1.843	1.708
Ti	0.022	0.024	0.043	0.048	0.028	0.031	0.011	0.010	0.041	0.039	0.032	0.037
Al	0.3:6	0.309	0.382	0.350	0.379	0.353	0.253	0.226	0.493	0.430	0.429	0.403
Fe	0.818	0.934	0.861	0.978	0.722	0.794	0.724	0.780	0.727	0.746	0.659	0.783
Mn	0.006	0.007	0.009	0.010	0.005	0.006	0.011	0.012	0.008	0.008	0.006	0.007
Mg	0.709	0.816	0.826	0.943	0.848	0.935	0.968	1.047	0.865	0.893	0.910	1.095
Ca	0.027	0.023	0.017	0.011	0.022	0.021	0.014	0.013	0.012	0.008	0.017	0.013
Na	0.032	0.009	0.019	0.000	0.025	0.012	0.012	0.007	0.018	0.007	0.021	0.010
K	0.021	0.000	0.023	0.000	0.035	0.000	0.017	0.000	0.029	0.000	0.027	0.000
Cr	0.002	0.002	0.001	0.001	0.000	0.001	0.001	0.001	0.001	0.001	0.002	0.002
X_{Mg}	0.46	0.47	0.49	0.49	0.54	0.54	0.57	0.57	0.54	0.54	0.58	0.58

* - average of 2 - 14 analyses corrected assuming all the K_2O in orthopyroxene represents contamination from surrounding glass. 7 kbar orthopyroxene analyses corrected using the composition of melt at 950° C; 10 kbar orthopyroxene analyses corrected using the composition of melt at 950° C for PON and 1000° C for KAI..

APPENDIX 8
Ilmenite Compositions

Run No.	RJ-9	RJ-25	RJ-31	RJ-10	RJ-26	RJ-32
n	23	4	8	6	4	8
P (kbar)	7	7	10	7	7	10
T (° C)	950	1000	1050	950	1000	1050
SiO_2	0.52	0.85	0.22	0.18	0.12	0.06
TiO_2	50.46	48.38	50.42	51.94	48.93	52.30
FeO	43.55	44.08	42.97	41.66	44.18	46.15
MnO	0.17	0.27	0.19	0.35	0.29	0.19
MgO	2.34	2.69	2.77	3.43	3.32	1.06
ZnO	0.10	0.07	0.04	0.04	0.07	0.05
Cr_2O_3	0.04	0.02	0.04	0.07	0.03	0.05
V_2O_3	0.00	0.05	0.03	0.05	0.02	0.02
Total	97.14	96.35	96.60	97.59	96.91	99.82
Cations 3 (O)						
Si	0.013	0.021	0.005	0.004	0.003	0.001
Cr	0.000	0.000	0.000	0.001	0.000	0.000
V	0.000	0.000	0.000	0.000	0.000	0.000
Fe^{3+}	0.042	0.099	0.054	0.026	0.133	0.025
Fe^{2+}	0.884	0.840	0.862	0.849	0.800	0.942
Mn	0.003	0.005	0.004	0.007	0.006	0.004
Mg	0.088	0.102	0.105	0.128	0.124	0.039
Zn	0.001	0.001	0.000	0.000	0.001	0.000
Ti	0.965	0.928	0.967	0.981	0.930	0.985

Fe^{3+} - calculated by charge balance.

APPENDIX 9
Glass Compositions*

Run No.	RJ-3	RJ-9	RJ-4	RJ-10	RJ-24
P (kbar)	7	7	7	7	10
T ($^{\circ}$C)	850	950	850	950	1000
SiO_2	73.06	71.78	72.22	71.78	74.65
TiO_2	0.20	0.42	0.64	0.98	0.47
Al_2O_3	15.03	14.96	12.25	14.21	14.2
FeO^T	1.38	2.02	1.93	2.22	2.09
MnO	0.02	0.01	0	0.05	0
MgO	0.22	0.32	0.70	0.61	0.35
CaO	1.83	1.63	1.24	0.78	1.03
Na_2O	2.70	2.84	2.88	1.19	1.22
K_2O	3.65	4.26	4.19	4.87	3.71
Total	98.09	98.24	96.05	96.69	97.72

* - Average of 1-3 analyses.